# Petrogenesis and magma chamber evolution of the Gawler Range Volcanics

Thesis submitted in accordance with the requirements of the University of Adelaide for an Honours Degree in Geology

Jade-Starr Tregeagle

November 2014


THE UNIVERSITY of ADELAIDE

# PETROGENESIS AND MAGMA CHAMBER EVOLUTION OF THE GAWLER RANGE VOLCANICS

## PETROGENESIS OF THE GAWLER RANGE VOLCANICS

## ABSTRACT

The Gawler Range Volcanics (GRV) have been extensively studied previously, but a source and emplacement mechanism has yet to be agreed upon. This study aims to constrain the source region of the GRV and to make deductions about how the GRV evolved. This has been done through a number of modelling techniques, including AFC modelling and use of the *Rhyolite-MELTs* program. The $\varepsilon_{Nd}$ values vary widely across the GRV, and these have been used in conjunction with trace element geochemistry to constrain the source region. It is deduced that the most primitive GRV basalts were the result of limited fractionation of a re-enriched refractory harzburgite source in the sub-continental lithospheric mantle. It is then shown that the entire GRV suite can be derived from one fractionation trend, however some assimilation is required.

## KEYWORDS

Petrogenesis; magma; evolution; Gawler Range Volcanics; *Rhyolite-MELTs*; AFC; modelling; geochemistry

**TABLE OF CONTENTS**

## LIST OF FIGURES AND TABLES

## INTRODUCTION

The Gawler Range Volcanics (GRV) and the co-magmatic Hiltaba Suite (HS) granites form a silicic-dominated large igneous province (SLIP), with a current preserved outcrop extent of about 25,000 $km^2$ (see Figure 1; Agangi et al. 2010). The Gawler SLIP also extends underneath younger formations in the northeast, giving a total minimum extent of 90,000 $km^2$ (McPhie et al. 2008), resulting in a total estimated volume for the Gawler SLIP of more than 100,000 $km^3$ (Kamenetsky et al. 2000) of which the volcanics potentially represent 25,000 $km^3$ (Agangi et al. 2012). The Gawler SLIP is located in the central portion of the Gawler Craton (GC) in South Australia (Kamenetsky et al. 2000) and occurred in an intracontinental setting during the final tectonothermal episode of the Gawler Craton development (Allen et al. 2003). The GRV have yielded U-Pb zircon ages in the range 1591±3 to 1592±3 Ma (Fanning et al. 1988, Agangi et al. 2012), which has contributed to the event being linked to Laurentian supercontinent assembly (Allen et al. 2008).

The GRV (see Figure 2) are composed of dominantly rhyolite and dacite lavas and minor pyroclastics, with basaltic magmas representing a small fraction of the provinces total volume (>90 vol. % of the succession is felsic; Agangi et al. 2012). The generally flat-lying GRV has been subdivided based on structural, stratigraphic, and geochemical features (Agangi 2011). The older Lower GRV (LGRV) is composed of small- to moderate- volume lava flows with diverse compositions from basalt through to rhyolite, and includes locally conspicuous ignimbrites (Kamenetsky et al. 2000). The LGRV comprises a number of sub-units, with the largest volume units (100 to 200 $km^2$) being the Yantea Rhyodacite, Lake Gairdner Rhyolite and Wheepool Rhyolite (Agangi 2011). Other significant units include Waganny Dacite and Bitalli Rhyolite (Allen et al. 2009).

Fractionation trends have previously been said to indicate that the felsic LGRV units are direct fractionates of the mafic units (Wade et al. 2012).

The more voluminous Upper GRV (UGRV) consists of extensive, gently dipping to flat lying, felsic lava flows and very minor ignimbrites (Agangi 2011). The UGRV is composed of at least three large volume (>1000 $km^3$), compositionally homogenous felsic massive lavas (Agangi et al. 2012) that are dacitic to rhyolitic in composition (Allen et al. 2003). The most extensive of these units (and the entire GRV) is the Yardea Dacite, which covers an area in excess of 12,000 $km^2$ (Giles 1988). The other main unit of the UGRV is the Eucarro Rhyolite. The LGRV are also known as the 'developmental phase' as there is a range of mafic to intermediate lavas, including at least 400 metres of subaerial basaltic lava flows (Giles 1988). The UGRV are thus termed the 'mature phase'.

There is evidence that the felsic magmas, including the Yardea Dacite, erupted at high temperatures (900 - 1100$^0$C), and were relatively dry and F-rich (Stewart 1994, McPhie et al. 2008, Allen et al. 2009, Agangi et al. 2012). The GRV are metaluminous to peraluminous, and alkali-calcic to calc-alkalic (Frost et al. 2001, Agangi 2011). Other geochemical signatures of the GRV include relatively high K, REE and HFSE concentrations, and the dacites and rhyolites have low Ca, Mg, Cr and Ni abundances compared to average crustal values or to Phanerozoic calc-alkaline rocks (Agangi 2011). Many authors have affiliated the GRV with anorogenic, A-type magmas based on these characteristics (Collins et al. 1982, Whalen et al. 1987, Giles 1988, Creaser and White 1991, Wade et al. 2012). The lower GRV also includes basaltic lava flows, including some very primitive compositions with high MgO and Cr and Ni (see Table

2). These are low Ti tholeiites and compared to MORB (see Table 2) the most primitive are poorer in $Na_2O$, CaO, $Fe_2O_{3(T)}$ and $TiO_2$.

In general, it has been largely accepted that in order to generate such large amounts of magma (both silicic and associated mafic) as are found in SLIPs, a mantle source of heat is required (Bryan et al. 2000, Agangi 2011). Previous petrographic studies of the GRV have shown that the more mafic magmas were derived from the mantle, while the silicic magmas were generated by fractional crystallisation and melting the crust (Allen et al. 2003, Allen et al. 2009). The initial $\varepsilon_{Nd}$ values of the LGRV are highly variable, ranging from of -7.4 to -1.6 in the Chitanilga Volcanic Province and -3.6 to +1.2 in the Glyde Hill Volcanic Province (Stewart 1994). This indicates that there was variable contribution of more than one magma source, which is also supported by the compositional variations across the GRV. The UGRV is relatively homogenous with

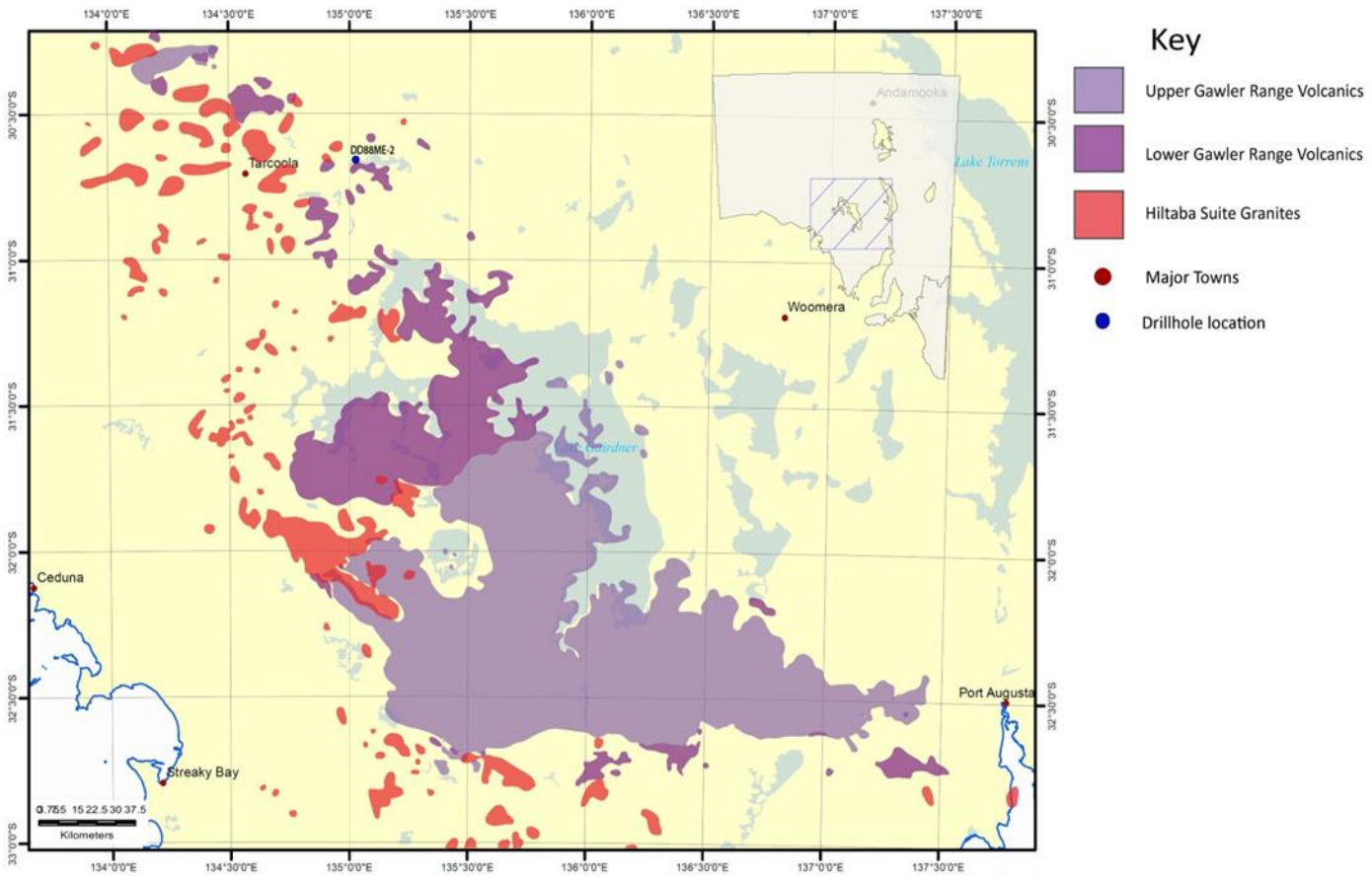


**Figure 1: A simplified geologic map of the total outcrop extent of the Gawler SLIP, showing the division between Upper and Lower Gawler Range Volcanics and the Hiltaba Suite granites.**

limited compositional variation. It has relatively constant $\varepsilon_{Nd}$ values between -3.8 and -4.5 (Stewart 1994). This further supports the idea that the magma must have had multiple sources that have mixed to different degrees. The lesser degree of variation in the UGRV may also indicate that the magma chamber was larger, and more homogenised.

Geothermometry, geobarometry and geochemical and isotopic modelling suggest that the Gawler SLIP originated by ponding of large volumes of mantle derived magma in the mid to lower crust. In order for assimilation and fractional crystallisation (AFC: DePaolo (1981)) processes to take a magma from the primitive source magma composition to the most siliceous felsic composition, it is possible that the total initial mass of the mafic parental magma may have been three to four times the extruded volume of dacites and rhyolites. The results of our calculations indicate that the most siliceous dacites and rhyolites resulted from up to 30% crustal digestion during crystallisation. The parental mafic magma was potentially produced from asthenospheric upwelling, either as a plume or due to decompression of the upper asthenosphere in lithospheric 'cracks' (rifts). At the same time, as later discussed in this paper, there is strong evidence that contaminated or enriched sub-continental lithospheric mantle (SCLM) also provided a separate source of mafic melts. The nature of the GRV parental magma will be assessed based on geochemical and isotopic evolution, with two main theories tested and presented: 1. a Mid-Ocean Ridge Basalt (MORB) parent contaminated by GC crust and 2. a partial melt of a depleted mantle (DM) parent with GC crustal contamination. These two possible sources will also be run through AFC models and comparisons made between the output and measured isotopic values to assess whether the GRV could be derived from pure fractional

crystallisation or combined AFC processes. Some calculations will then be made to estimate the volume of mafic parental magma that would have been required to produce the extruded volume of GRV.

A range of geothermometric and geobarometric methods will be used to estimate temperatures (T) and pressures (P) of the stages of magmatic evolution. The Rhyolite-MELTs program developed by Gualda et al. (2012) will also be used to model liquid evolution trends from potential parental basalts that are represented in the LGRV. The quality of the Rhyolite-MELTs models will be assessed through direct comparison with the GRV lavas and their trends, and by correlation of the P-T conditions in the Rhyolite-MELTs models with the values obtained from the samples through geobarometry and geothermometry.

## METHODS

The work done by Stewart (1994) was used as the starting point for this study. The geochemical analyses run by Stewart (1994) covered a range of rock types and locations within the GRV, however there was less data for the LGRV and successions showing variations in magma composition. The main goal of this study was to further develop the work of Stewart (1994), particularly by filling in these gaps. New data was obtained by geochemical analysis of samples taken from drill core made available by DMITRE (now the Department of State Development). The drillhole DD88ME-2 was chosen as a source of new sample data as it showed variation in lithology, with interlayering of pyroxenites, andesites, and dacites (noting that the relationships between the lithologies in this hole are quite enigmatic). Eighteen samples were collected from the core and whole rock geochemistry was obtained using XRF and Solution ICP-MS.

More recent work into modelling programs, such as that done by Gualda et al. (2012) into the program Rhyolite-MELTs, was then utilized to assess the magma chamber evolution and possible source compositions. The program Rhyolite-MELTs generates models of magma chamber evolution over different pressure and temperature space, based on the input of geochemical data. The program predicts the mineral assemblages one might expect to form under the varying circumstances. Other temperature and pressure modelling was done using a variety of geothermometric and geobarometric programs such as those developed by Putirka (2008) (T-dependency of feldspar-melt and olivine-melt relations; P-dependency of site substitution in clinopyroxene (Nimis 1999), zircon saturation temperatures (Watson 1979) and P-dependency of peridotite melts (Lee et al. 2009)) to compare to the Rhyolite-MELTs output. Additional modelling into possible source magmas was conducted, with particular interest in comparing mid-ocean ridge basalts (MORB) with the most primitive GRV units and assessing the levels of contamination from Gawler Craton crust.

## OBSERVATIONS AND RESULTS

### Core samples

The target core was selected in a quest to access more mafic lavas from the LGRV in order to provide more evidence for petrogenetic modelling. The drill hole selected was indeed composed of interlayered felsic lavas and mafic (or in fact ultramafic) rocks. As it turned out many of the mafic horizons turned out to be cumulate-textured pyroxenites. These are relatively fresh with fresh pyroxenes and sometimes olivine. They also seem to be undeformed, suggesting they post-date the main orogenic events experienced by the Gawler craton. Prior MESA/ DMITRE interpretation has assigned these rocks to the

Lower GRV. Of the eighteen samples taken from the core, ten were from pyroxenite layers that had very similar geochemistry despite being interlayered between other igneous rock types, including dacites and andesites. A brief description of the sample depths, rock types and features can be found in Table 1. For a full core log, including descriptions of layers not sampled, see Appendix B.

Contacts between each rock type were difficult to describe due to the limited width of the core and the core being broken up in many places. As such, it is difficult to draw conclusions about the nature of the succession and exactly how the rocks are structurally related to each other.

The pyroxenites have lower $TiO_2$, $Al_2O_3$, $Na_2O$, and $K_2O$ than the other core samples, and higher FeO, MgO, and CaO. They are also very high in Cr, with values similar to or higher than a small range of primitive mafic GRV rocks previously analysed.

**Table 1: Summary of drill core samples**

| Sample depth from-to (m) | Sample number | Rock type | Features |
|---|---|---|---|
| 73.2-73.3 | 2067545 | Porphyritic dacite/ rhyodacite | Phenocrysts of plagioclase, k-spar<br>Fine laths of hornblende and biotite<br>Fine quartz groundmass |
| 77.05-77.15 | 2067546 | Porphyritic dacite | Similar to 2607545 |
| 85.5-85.6 | 2067547 | Pyroxenite | 40% plagioclase, 25-30% amphibole, some magnetite, pyroxene<br>Intercumulate mica (?) |
| 97.05-97.15 | 2067548 | Vesicular/ amygdaloidal basalt | Irregular vesicles, some filled<br>Quartz pieces remnants of crystal digestion (?)<br>Fresh pyroxenes |
| 99.8-99.9 | 2067549 | Hornblendite | K-spar phenocrysts, amphibole needles<br>Lamprophyric<br>Delicately preserved texture |
| 106.5-106.6 | 2067550 | Pyroxenite | Similar to 2067547<br>Massive to very weakly foliated |
| 119.05- | 2067551 | Porphyritic andesite | Zoned plagioclase phenocrysts |

| | | | |
|---|---|---|---|
| 119.1 | | | Amphibole phenocrysts look original<br>Looks like typical GRV andesites/ dacites in thin section |
| 125-125.1 | 2067552 | Porphyritic andesite | Very similar to 2067551 |
| 135.7-135.8 | 2067553 | Pyroxenite | Similar to previous pyroxenites<br>Intercumulate clinopyroxene |
| 145.4-145.5 | 2067554 | Alkali dolerite (?) | Distinct amphibole needles<br>Chilled upper contact with andesite layer |
| 156.35-156.4 | 2067555 | Andesite | K-spar, plagioclase and rare biotite laths in quartzose groundmass<br>Indistinct lower contact (with sample 2067556) |
| 166.15-166.25 | 2067556 | Pyroxenite | Equigranular plagioclase, olivine (?)<br>Laths of biotite |
| 201.5-201.6 | 2067557 | Pyroxenite | Rare xenoliths of quartz-k-spar porphyry and k-spar-quartz-biotite gneiss |
| 218.8-218.9 | 2067558 | Pyroxenite | |
| 223.8-223.9 | 2067559 | Pyroxenite | |
| 247.5-247.6 | 2067560 | Pyroxenite | |
| 267.1-267.2 | 2067561 | Pyroxenite | |
| 297.8-297.9 | 2067562 | Pyroxenite | Cumulative texture |

## Geochemistry

Overall, the developmental phase GRV show a much greater compositional diversity than the mature phase GRV. The high-silica samples from the drill core tend to plot on the same trend as the main body of existing GRV data (see Figures 2 and 3), close to the Yardea Dacite values. Other core samples, particularly the pyroxenites, appear to continue the trends into lower silica values. MORB values have been included in all geochemical plots for comparison.

The pre-existing GRV data as well as the new analyses reported here are displayed on a TAS diagram (see Figure 2). This shows a positive correlation between total alkalis and silica and also shows that the GRV extends from basalts through andesites to dacites and rhyolites. In the Harker diagrams (see Figure 3), the GRV data define coherent trends consistent with crystal-liquid fractionation. Close inspection of these broad trends also tend to reveal discrete sub-trends. CaO, FeO, and MgO all decrease with increasing $SiO_2$, while $K_2O$ shows continuous enrichment. $Al_2O_3$, $Na_2O$, $P_2O_5$ and $TiO_2$ each show inflected trends with initial enrichment followed by a change to depletion at around 60% $SiO_2$. While there is a large gap between their compositions and those of the GRV, the pyroxenites consistently fall on the extrapolation of the mafic GRV basalt towards more primitive end-members. As discussed later, their orthopyroxene (OPX)-clinopyroxene (CPX) ± olivine mineralogies are those predicted by *Rhyolite-MELTs* simulations to explain the early stages of GRV fractionation of primitive basaltic parent magma. This is also consistent with their cumulate textures. The intermediate core samples fall on the GRV trends, clustering around the low silica end of the mature phase (like some Yardea dacites).

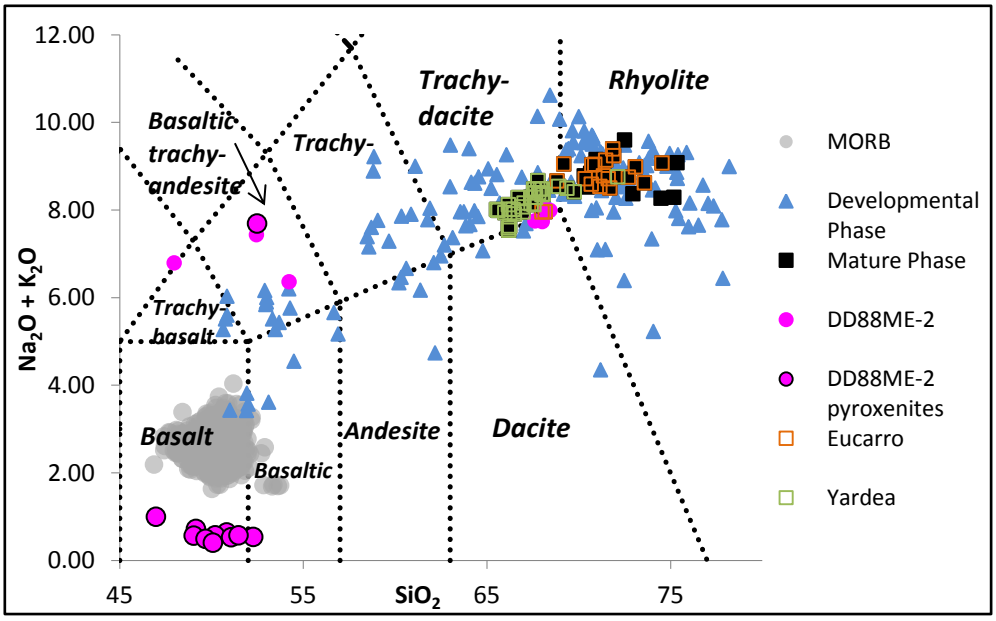


**Figure 2: Total alkali vs. $SiO_2$ (TAS) plot for the GRV (data from Stewart (1994)), samples from drillhole DD88ME-2, and MORB (data from Melson et al. (2002)) for comparison. IUGS classification (from Le Bas et al. (1986)) is shown in black dotted lines with the fields labelled in italics.**

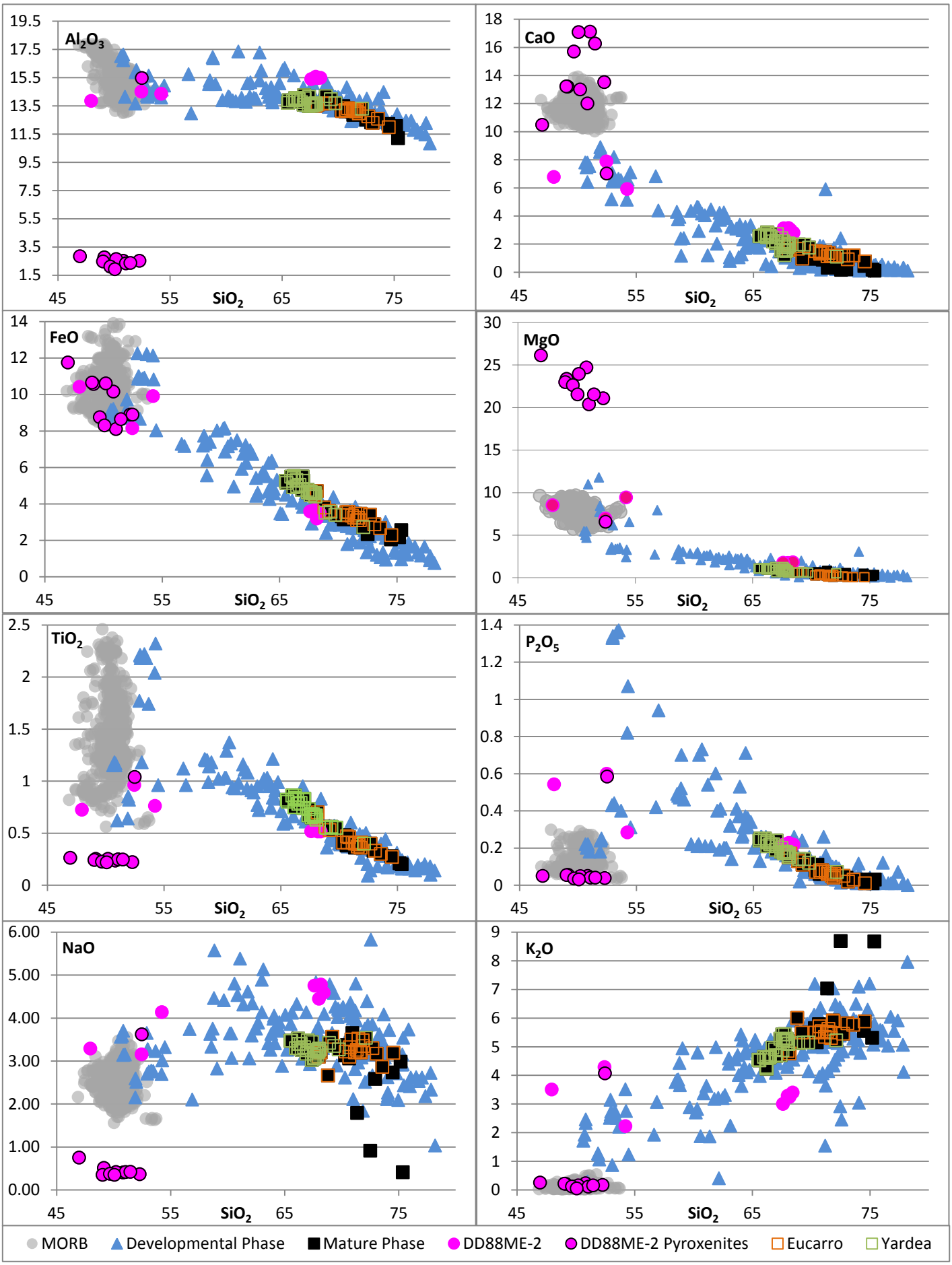


**Figure 3: Harker diagrams – variation of major elements vs. $SiO_2$ for the GRV (data from Stewart (1994)), samples from drillhole DD88ME-2, and MORB (data from Melson et al. (2002)) for comparison.**

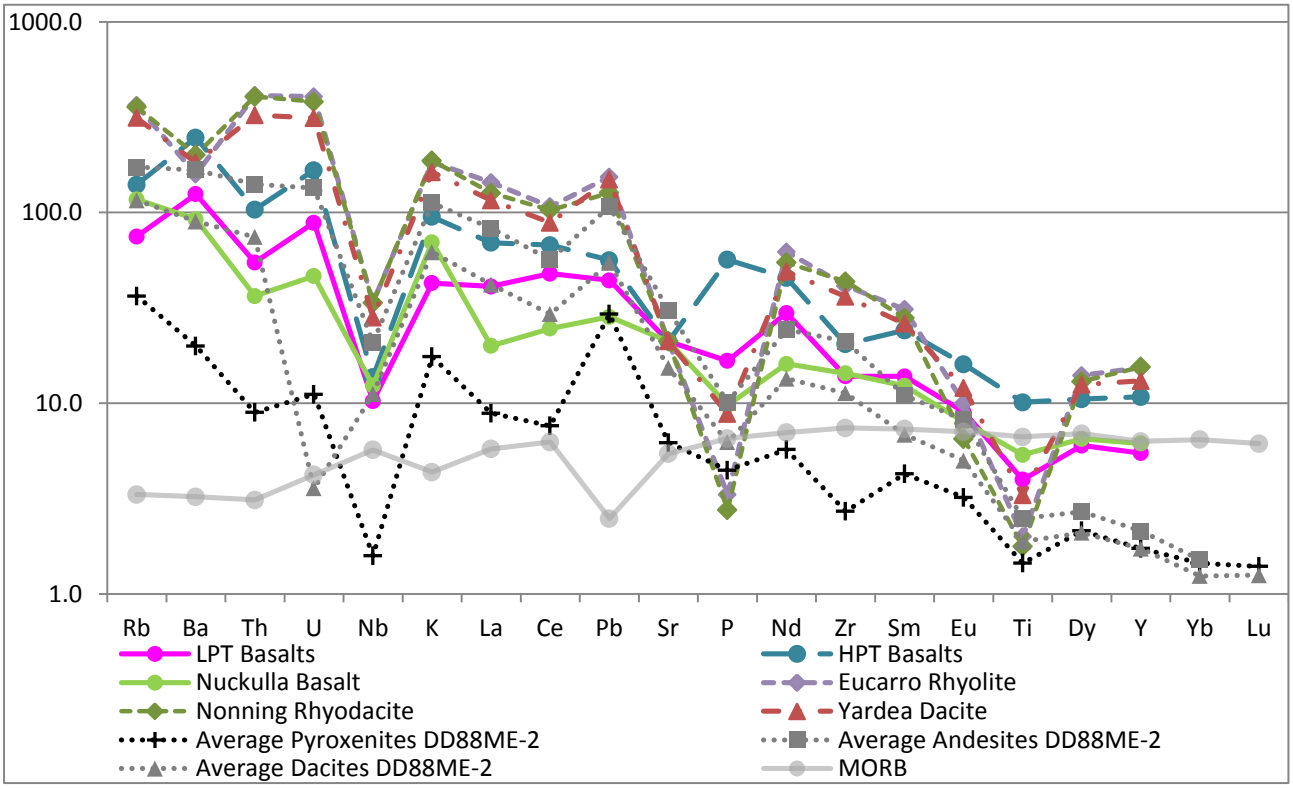


**Figure 4: Primitive mantle normalised spidergram showing averages for three types of rock found in the core, and a selection of Upper and Lower GRV units (GRV data from Stewart (1994)). Normalising values are from Sun and McDonough (1989).**

The available trace element data for the existing GRV dataset was not as extensive as what we analysed for in the core samples, however comparisons can still be made based on what is available, and overall trends. The primitive mantle normalised (PMN) spidergram (normalising values from Sun and McDonough (1989)) can be found in Figure 4. A selection of rock types from the GRV are plotted with averages of the three most abundant rock types found in the core – pyroxenite, dacite, and andesite. Large ion lithophile elements (LILE) are on the left of the figure, and high field strength elements (HFSE) on the right. These all show a negatively sloping trend. For most of the available elements, the GRV and core dacites and andesites appear to be relatively similar, except for a difference in Y. As with most of the GRV rocks, the core samples show distinct Nb and Sr depletions, and strong Pb enrichments.

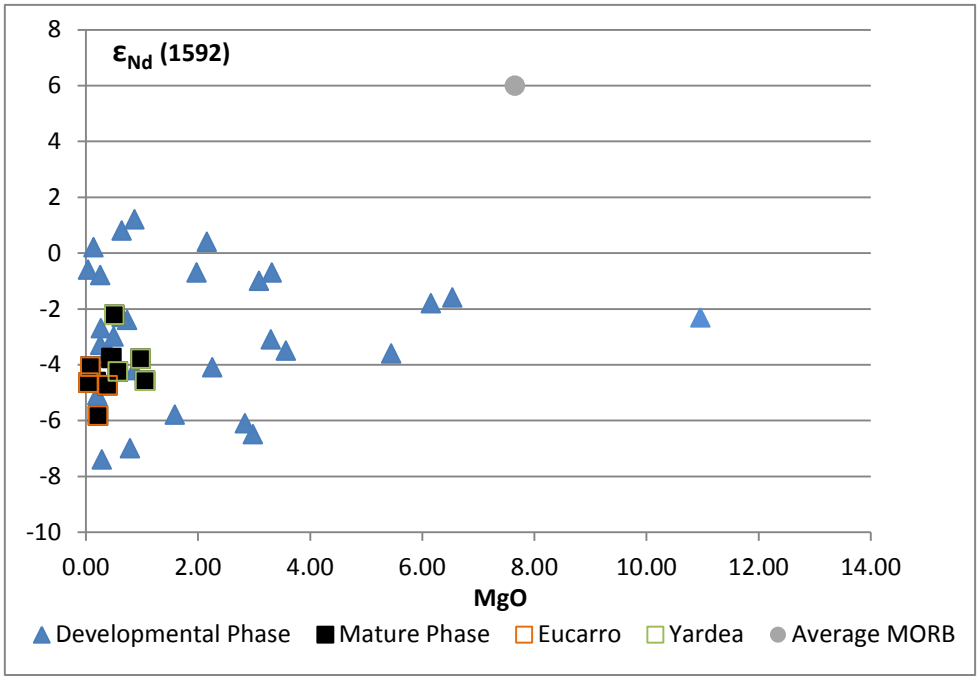


**Figure 5: $\varepsilon_{Nd}$ (1592) vs. MgO for the available GRV data (Stewart 1994), with average MORB plotted for comparison (Melson et al. 2002).**

## ISOTOPES

Figure 5 shows the available $\varepsilon N_d$ data at 1592 Ma versus MgO wt.%. This data was not collected for the core rocks, so only the previously analysed GRV data is presented, with comparison to average MORB. There is a significant degree of variation between the $\varepsilon_{Nd}$ values (+1.2 to -7.4) for the GRV. It is noted that MORB $\varepsilon_{Nd}$ at 1592 Ma was +6 and GC crustal values down to about -15 (Stewart 1994). There is a general trend towards lower $\varepsilon_{Nd}$ with decreasing MgO, as the magmas become more felsic.

## REE PATTERNS

Rare earth element (REE) patterns for the drill core samples and three mature phase GRV rocks are presented in Figure 6. The core samples seem to have somewhat different REE patterns than those from the GRV (noting that there is very limited REE data on the GRV rocks). The drill core rocks are significantly more depleted in the middle to heavy REE (M-HREE). The drill core samples therefore have significantly higher La/Yb and Sm/Yb ratios that the GRV. On the other hand, the La/Sm values for both suites are similar. Whereas the mature phase GRV have a negative Eu anomaly, this is also not evident in the core samples. The more felsic core rocks are more similar to the GRV, except in the HREE that are noticeably more depleted than the core rocks. The Eucarro and Nonning Dacites have almost identical REE and PMN trace element patterns. Interestingly, although the pyroxenites are texturally cumulate rocks dominated by clinopyroxene and orthopyroxene, they are nevertheless LREE-enriched and have the same MREE-HREE depletion seen in the felsic lavas from the drill core. It has to be said that the samples from the drill core remain an intriguing issue. Are they

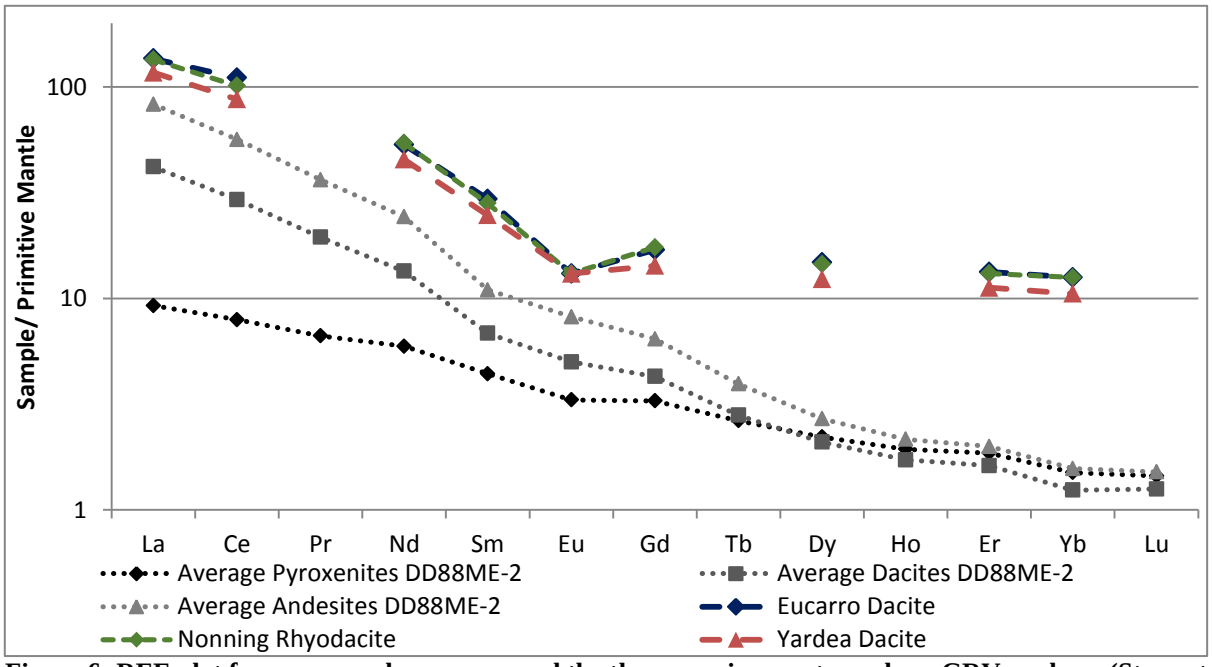


**Figure 6: REE plot for core sample averages and the three previous mature phase GRV analyses (Stewart 1994). These are primitive mantle normalised (normalising values from Sun and McDonough (1989)).**

really part of the lower GRV as prior interpretation would have it, or are they unrelated?

**Table 2: compositional comparisons between primitive GRV basalts and MORB, with the calculated primary melt compositions for the GRV basalts (based on supplementary program from Lee et al. (2009)).**

| | Average MORB | Primitive GRV Basalt K8 | Most primitive GRV Basalt K101 | GRV Basalt K110 | GRV basalt K33 | Calculated primary melt composition K101 | Calculated primary melt composition K110 | Calculated primary melt composition K33 |
|---|---|---|---|---|---|---|---|---|
| **$SiO_2$** | 50.45 | 51.00 | 51.91 | 51.94 | 52.01 | 51.82 | 50.43 | 50.07 |
| **$TiO_2$** | 1.44 | 0.62 | 0.64 | 0.85 | 0.82 | 0.63 | 0.72 | 0.68 |
| **$Al_2O_3$** | 15.31 | 14.14 | 13.65 | 15.87 | 16.02 | 13.36 | 13.37 | 13.34 |
| **$FeO_{(T)}$** | 10.26 | 8.66 | 8.69 | 9.16 | 9.71 | 8.73 | 9.53 | 9.89 |
| **MgO** | 7.65 | 10.96 | 11.77 | 7.72 | 8.44 | 12.75 | 14.45 | 15.00 |
| **CaO** | 11.67 | 7.54 | 8.55 | 8.88 | 8.62 | 8.37 | 7.48 | 7.19 |
| **$Na_2O$** | 2.52 | 3.15 | 2.15 | 2.56 | 2.51 | 2.11 | 2.18 | 2.09 |
| **$K_2O$** | 0.13 | 0.28 | 1.27 | 1.23 | 1.06 | 1.24 | 1.04 | 0.88 |
| **$P_2O_5$** | 0.14 | 0.18 | 0.18 | 0.24 | 0.25 | | | |
| **La** | 3.96 | 27.0 | n.d. | n.d. | n.d. | | | |
| **Ce** | 11.12 | 66.0 | 78.0 | 54.0 | 58.0 | | | |
| **Ba** | 22.59 | 492.0 | 1005.0 | 842.0 | 718.0 | | | |
| **Rb** | 2.11 | 9.7 | 45.0 | 42.0 | 36.0 | | | |
| **Cr** | 269.41 | 941.0 | 1050.0 | 619.0 | 600.0 | | | |
| **Ni** | 108.13 | 289.0 | 362.0 | 197.0 | 192.0 | | | |
| **Sc** | 42.03 | 31.0 | 29.0 | 32.0 | 30.0 | | | |
| **$\varepsilon_{Nd}$** | +6 | -1.88 | n.d. | n.d. | n.d. | | | |

**Table 3: the un-normalised trace element compositions of average GRV basalt, MORB, depleted mantle and GC crust used in modelling, with contamination values for MORB +25% GC crust and DM + 5% GC crust. These values were used to indicate how well the modelled contamination could suit the observed GRV data.**

| | Av GRV Basalt | GC crust | MORB | MORB + 25% GC | Depleted Mantle | DM +5% GC |
|---|---|---|---|---|---|---|
| **Rb** | 32.38 | 118.77 | 2.108910122 | 31.275 | 0.0800 | 6.01 |
| **Ba** | 492 | 650.52 | 22.59766514 | 179.579 | 0.9080 | 33.39 |
| **Th** | 4.35 | 28.12 | 0.264192041 | 7.228 | 0.0160 | 1.42 |
| **U** | 1 | 3.00 | 0.088480735 | 0.816 | 0.0072 | 0.16 |
| **Nb** | 5.92 | 9.72 | 4.063180441 | 5.477 | 0.3456 | 0.81 |
| **K** | 7803.397028 | 28673.98 | 1087.901774 | 7984.421 | 200.0000 | 1623.70 |
| **La** | 32 | 59.13 | 3.960869986 | 17.752 | 0.5360 | 3.47 |
| **Ce** | 64.4 | 105.25 | 11.11547216 | 34.649 | 1.6840 | 6.86 |
| **Pb** | 12.2 | 22.61 | 0.46385136 | 6.000 | 0.1360 | 1.26 |
| **Sr** | 539.86 | 172.26 | 114.8313747 | 129.189 | 24.3680 | 31.76 |
| **P** | 1125.96689 | 367.78 | 620.7108134 | 557.479 | 160.0000 | 170.39 |
| **Nd** | 34 | 37.35 | 9.508429064 | 16.468 | 1.9320 | 3.70 |
| **Zr** | 121.58 | 229.45 | 83.08697881 | 119.677 | 17.0760 | 27.69 |
| **Sm** | 5 | 8.01 | 3.249083409 | 4.440 | 0.8400 | 1.20 |
| **Eu** | 1.2 | 1.15 | 1.190238113 | 1.179 | 0.3440 | 0.38 |
| **Ti** | 4927.884856 | 2960.19 | 8651.013813 | 7228.309 | 3560.0000 | 3530.01 |
| **Dy** | 3 | 3.22 | 5.10481303 | 4.634 | 1.8840 | 1.95 |
| **Y** | 22.62 | 22.13 | 28.70840833 | 27.063 | 12.5160 | 13.00 |
| **Yb** | 1.2 | 1.50 | 3.176753358 | 2.757 | 1.3920 | 1.40 |

## DISCUSSION

The project utilised the geochemical and isotopic data from Stewart (1994). Her data showed that the GRV extended from basalts, through andesites to dacites and rhyolites and, though often referred to as "bi-modal", it in fact has representation over the entire silica range. However, of course, the volumetric representation is hugely skewed towards the dacites and rhyodacites. Stewart (1994) identified two basaltic sub-groups; 1. low phosphorous and titanium (LPT) basalts and 2. the high phosphorous and titanium (HPT) basalts and basaltic andesites. These lavas are the most primitive of the GRV and plot at the lowermost $SiO_2$ range of the Harker diagrams in Figure 3. These GRV basalts are comparatively enriched in most lithophile trace elements presented in the PMN spidergram plot although most have lower Ti (see Figure 4) and other HFSE. The most primitive LPT basalts have very high compatible trace element (Ni, Cr, Sc) concentrations, but also have high LILE/HFSE ratios, LREE enrichment. At the same time, these basalts (from outcrops in the Kokatha area) range up to samples with very high MgO (> 11%), the highest values of the GRV. Their MgO, Cr and Ni values are high compared to MORB (values for which are from Jenner and O'Neill (2012) and Melson et al. (2002)), but the values for CaO, $Na_2O$, $TiO_2$, $FeO_{(T)}$ are lower. This indicates a refractory mantle source with little or no CPX. Clearly the most MgO-rich of these samples (e.g. K101) have undergone almost no fractionation to produce the earliest GRV. This compositional comparison is summarised in Table 3. Compared to MORB, the GRV basalts also have higher $K_2O$ , LREE, Pb, Rb, Ba, U and Th. Tellingly, although MORB at 1592 Ma had an $\varepsilon_{Nd}$ value of about +5.9, the GRV basalts fall in the range -1 to -3.

In order to be able to make assessments about the potential source of the GRV, Stewart (1994) identified the geochemical and isotopic characteristics of some potential crustal source lithologies. Stewart (1994) concluded that the trace element geochemistry of the GRV basalts could not be achieved from asthenospheric basalts (e.g. MORB) alone. In particular, she inferred that the LREE enrichment and high LILE/HFSE ratios must have been derived from the continental lithosphere (Stewart 1994). These conclusions are further explored here.

## Source

It is clear that the GRV suite includes small volumes of very primitive basalt. The preceding discussion drew attention to characteristics which on the one hand suggested a very refractory (harzburgite) mantle source, but at the same time showed lithophile crust-like features. The obvious question is whether the basaltic potential parents to the GRV are MORB-type mantle melts that have been contaminated by continental crust as they ascend, or melts of a refractory harzburgite mantle that has been contaminated by crustal material (either due to prior subduction processes or due to basal crustal delamination)? Both these models are tested below. Both these options have been modelled using the equations of DePaolo (1981) by mixing the parent composition with progressively greater amounts of Gawler Craton Archean crust. The isotopic compositions of each component at 1590 Ma were considered as an indication of how similar to the GRV data the potential parent would become. These models are based on pure fractional crystallisation of the parent magmas and are used to give an indication of what the source composition may have been prior to partial melting. A further test was then applied to assess if partial melting of that source could produce the trace element patterns of a primitive GRV basalt (using the equations of Shaw (1970) and Greenland

(1970)). A summary of the values used to produce the PMN spidergrams used as an indicator for how well the model suits the GRV data can be found in Table 3.

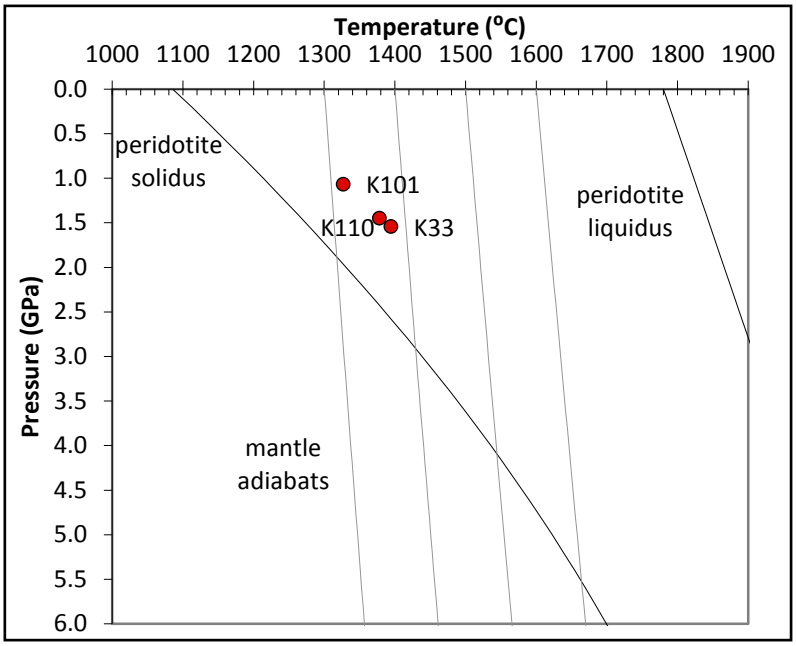


**Figure 7: the calculated pressure and temperature conditions of melt segregation from the mantle for three of the most primitive GRV basalts. Based on the calculations of Lee et al. (2009).**

## MANTLE MELTING CONDITIONS

The routine of Lee et al. (2009) was used to assess the primary magma composition of the GRV. Based on silica activities, this calculates the pressure (and temperature) at which basaltic melts can be derived by partial melting of a peridotite source. The results of these calculations are summarised in Table 2 and Figure 7. The diagram in Figure 7 also shows a range of adiabats for different mantle potential temperatures (the steep grey lines). Normal MORB asthenosphere would be close to the coolest of these adiabats, reaching surface pressures at about $1300^0$C. These calculations imply that the most primitive GRV LPT basalt is very near to a primary melt (i.e. has experienced very little fractionation) and must have been derived by very shallow melting (approximately 1.6 GPa, which is equivalent to about 50 km depth) and around $1360^0$C. This is a depth in the mid to upper levels of the SCLM where temperatures are more likely to be around $850^0$C. If indeed (as discussed below), the parental GRV basalts are derived from contaminated harzburgitic SCLM and not the result of simple crustal contamination of

MORB-like melts, then these pressure-temperature results pose some interesting geodynamic/ tectonic questions as to how such high temperature melting occurred well inside the SCLM.

*Option One – MORB-like parent with contamination from Gawler Craton Archean crust?*

For this model, a mantle derived basalt with MORB composition and crustal contamination from GC Archean crust was simulated. The primary outcome of this modelling is shown in Figure 8. This model was able to produce an εNd value comparative to the primitive GRV basalts only after 15-20% addition of GC Archean crust. The PMN trace element trends (see Figure 9) also do not match up with those of the GRV basalts. While some elements are similar, key differences occur in other elements. Some of the modelled values are too high for the GRV basalts, such as Th, Ti and Yb; while others are too low, such as Ba, Pb and Nd. Ultimately, regardless of how

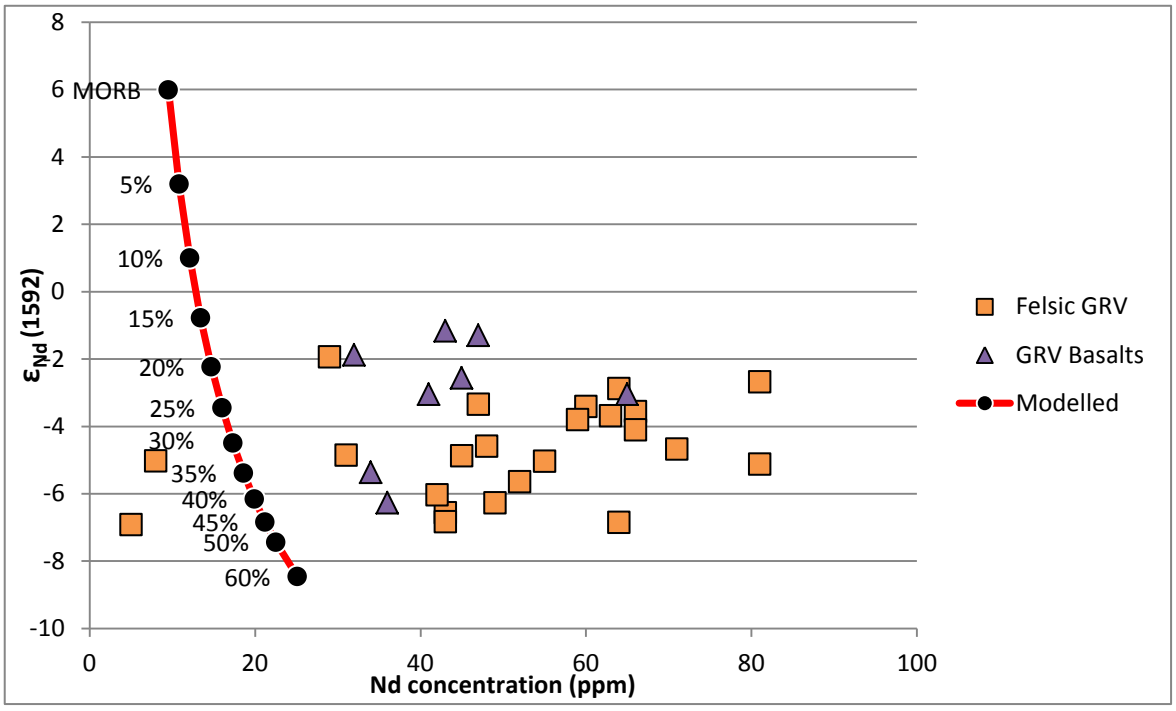


**Figure 8: Option One – $\varepsilon_{Nd}$ vs. concentration Nd modelling from MORB source composition compared with actual GRV data. Percentages are the amount of Gawler Craton crustal contaminant added to the MORB source composition.**

well the trace element data fits, this model would result in a bulk composition that is much more siliceous than the primitive GRV basalts. It therefore cannot be considered a feasible model for the GRV source.

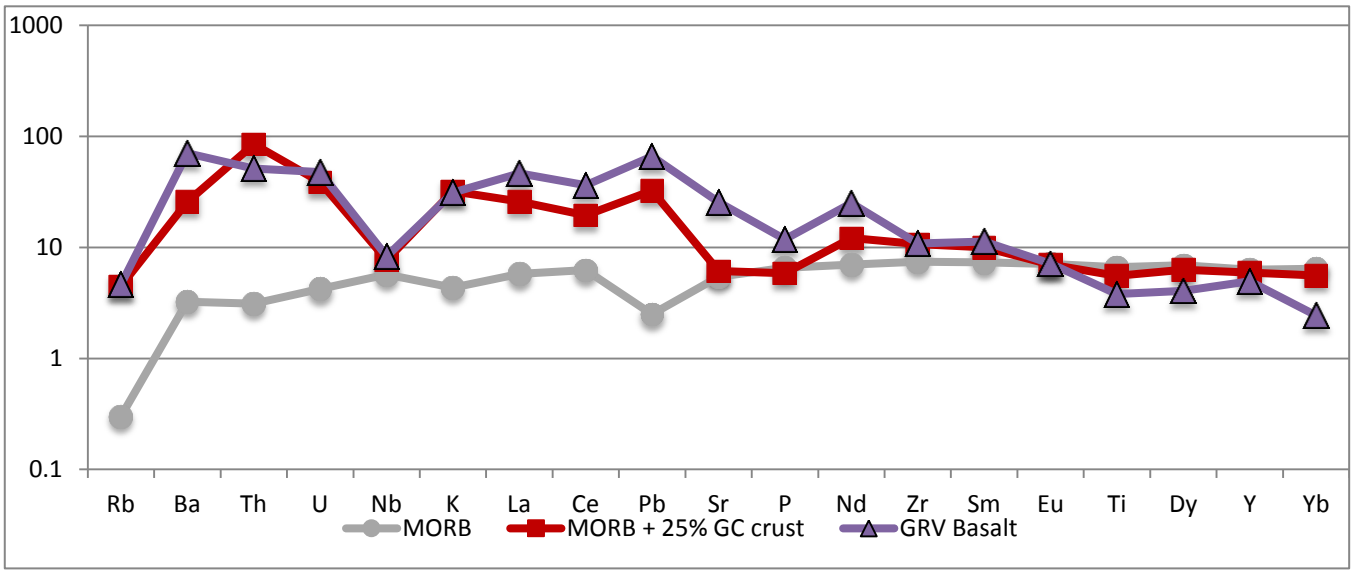


**Figure 9: PMN trace element patterns for MORB, a primitive GRV basalt and the modelled MORB + 25% Gawler Craton crustal contamination.**

*Option Two – Depleted Mantle source with contamination from Gawler Craton Archean Crust?*

This model involved the mixing of a depleted mantle peridotite source and the GC Archean crust at 1590 Ma. The primary output of this model can be found in Figure 10. Under this model, obtaining a composition that is isotopically like the most primitive GRV requires around 5% addition of crustal material. However, this resultant composition has a much lower concentration of Nd than the GRV (3.68 ppm versus 32 ppm for the GRV). This disparity is related to the affinities of Nd and can be accounted for by melting the contaminated source by about 15%. Most importantly, the εNd values are similar without the modelled melt becoming more siliceous than the most primitive GRV.

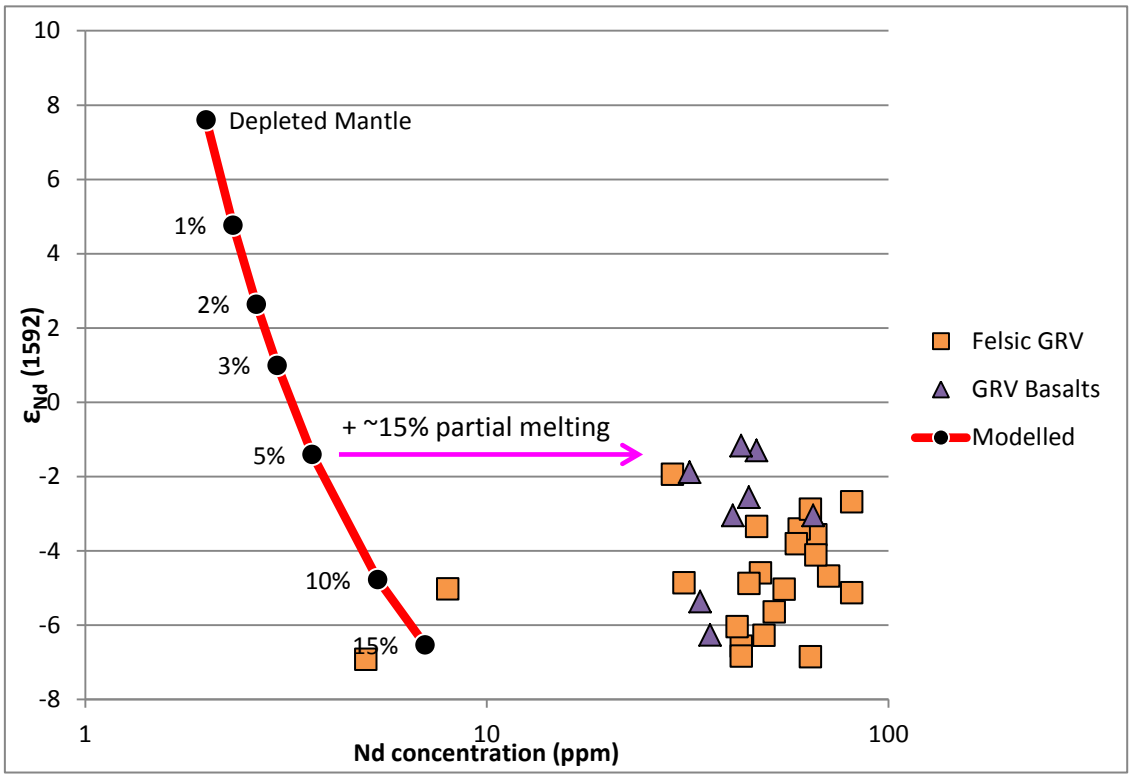


**Figure 10: Option Two – $\varepsilon_{Nd}$ vs. concentration Nd modelling from a depleted mantle source compared with observed GRV data. Percentages are the amount of Gawler Craton crustal contaminant added to DM source composition. The pink arrow indicates the difference in concentration that would be achieved with approximately 15% partial melting of the contaminated DM source (that includes 13% garnet).**

The partial melting modelling also shows that there must have been around 13% garnet in the depleted mantle source in order for the trace element signatures to be replicated. This was based on the distribution coefficients of a number of trace elements in typical peridotite minerals (values from Rollinson (1993)). The partial melting model is summarised in Table 4. As this table shows, the percentages of the minerals olivine (Ol), orthopyroxene (OPX), clinopyroxene (CPX) and garnet (Gar) were able to be altered, as was the fraction of melting. The values presented here are the final amounts that were required to achieve the PMN trace element pattern that best fit the GRV data (see Figure 11).

The PMN spidergram (see Figure 11) shows that the trace element signatures for the GRV can be replicated reasonably well in this model. While the pure depleted mantle

pattern is quite far off, it at least begins with lower concentrations in the HFSE than the GRV, which then allows the crustal contaminant to alter these concentrations only so much that they match the GRV. This is opposed to the MORB-like source in which the HFSE concentrations start higher than the GRV values, and cannot be brought down by the addition of crustal contaminant. The addition of only 5% crust to the depleted mantle source reasonably accurately replicates the pattern observed in the GRV. The Pb peak is evident, as is the Nb depletion. The result of about 15% partial melting of this depleted mantle source is that the LILE concentrations are increased in the melt, with little effect on the HFSE element concentrations. This results in the final PMN pattern very closely matching the observed GRV pattern.

**Table 4: summary of partial melting modelling for the depleted mantle + 5% GC crustal contamination**

| | Kd Values | | | | Ol:OPX:CPX:Gar | Fract. Melting |
|---|---|---|---|---|---|---|
| Partial Melting Model | Ol | Opx | Cpx | Gar | 39:40:8:13 | 0.15 |
| Rb | 0.0100 | 0.0220 | 0.0310 | 0.0420 | 0.02064 | 35.89861486 |
| Ba | 0.0100 | 0.0130 | 0.0260 | 0.0230 | 0.01417 | 206.0465558 |
| Th | 0.0100 | 0.0200 | 0.0300 | 0.0100 | 0.0156 | 8.704792628 |
| U | 0.0100 | 0.0050 | 0.0150 | 0.0050 | 0.00775 | 1.001612517 |
| Nb | 0.0100 | 0.0130 | 0.0260 | 0.0230 | 0.01417 | 5.024943423 |
| K | 0.0100 | 0.0130 | 0.0260 | 0.0230 | 0.01417 | 10020.0806 |
| La | 0.0070 | 0.0200 | 0.0560 | 0.0010 | 0.01534 | 21.25585494 |
| Ce | 0.0060 | 0.0220 | 0.0920 | 0.0070 | 0.01941 | 41.21571999 |
| Pb | 0.0140 | 0.0130 | 0.0260 | 0.0230 | 0.01573 | 7.710354345 |
| Sr | 0.0140 | 0.0130 | 0.0260 | 0.0230 | 0.01573 | 194.4214519 |
| P | 0.0140 | 0.0130 | 0.0260 | 0.0230 | 0.01573 | 1042.961902 |
| Nd | 0.0060 | 0.0280 | 0.1800 | 0.0260 | 0.03132 | 20.96460552 |
| Zr | 0.0070 | 0.0500 | 0.2500 | 0.1020 | 0.05599 | 140.1608313 |
| Sm | 0.0070 | 0.0500 | 0.3400 | 0.1020 | 0.06319 | 5.883820719 |
| Eu | 0.0070 | 0.0500 | 0.4740 | 0.2430 | 0.09224 | 1.681559868 |
| Ti | 0.0130 | 0.2000 | 0.5820 | 1.9400 | 0.38383 | 7412.008332 |
| Dy | 0.0130 | 0.2000 | 0.5820 | 1.9400 | 0.38383 | 4.096120675 |
| Y | 0.0300 | 0.2000 | 0.6000 | 3.0000 | 0.5297 | 21.65214019 |
| Yb | 0.0490 | 0.3400 | 0.5420 | 5.0000 | 0.84847 | 1.603794538 |

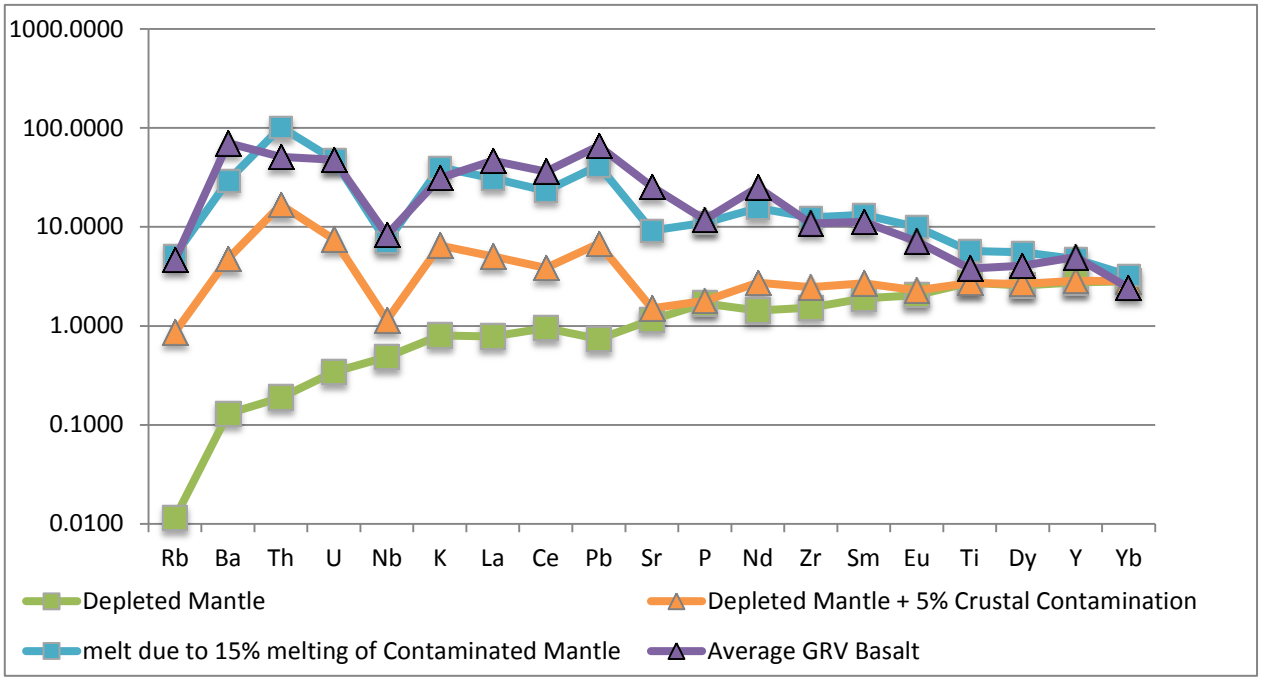


**Figure 11: PMN trace element patterns for depleted mantle, primitive GRV basalt and the modelled results of DM + 5% GC crustal contamination and 15% melting of that magma.**

Of these two options for the GRV source magma, the contaminated depleted mantle model seems to be the most likely. This model requires much less total contamination and crystallisation to reach the observed data points. It has also been noted by a number of authors (Francis 2003, Griffin et al. 2003, Arndt et al. 2009) that the sub-continental lithospheric mantle (SCLM) beneath Archean cratons is typically depleted. This further supports the idea that the GRV source may have been a contaminated depleted mantle as it is highly likely that a form of depleted mantle exists beneath the Gawler Craton.

### *Rhyolite-MELTs* modelling

The most primitive LPT basalt was used as the starting bulk composition of the magma chamber for the purpose of the *Rhyolite-MELTs* modelling. It was found that a single fractional crystallisation trend is able to produce the geochemistry of the GRV from developmental to mature phase. This is shown in the second set of Harker diagrams in

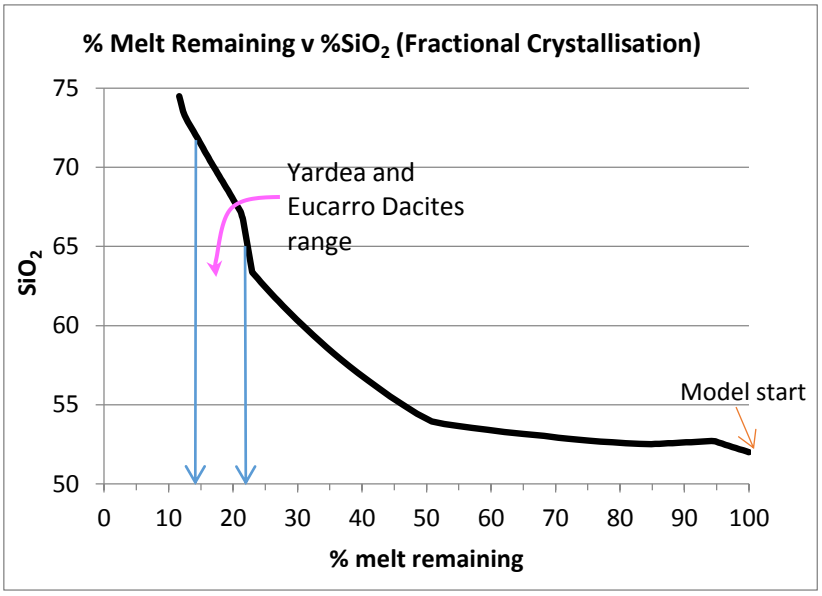


**Figure 12: The fractional crystallisation trend of the GRV as modelled by Rhyolite-MELTs. The blue arrows show the range of $SiO_2$ that is observed in the most voluminous felsic GRV units, the Eucarro and Yardea Dacites, and indicate how much of the remaining melt they would represent under this model (approx. 14-20%).**

Figure 14 in which the major element oxide outputs from the model are plotted with the actual GRV data. In order for the most siliceous compositions to be reached a two-stage model needed to be devised. In the first stage, the most primitive LPT basalt was crystallised under three kbar of pressure. This resulted in a dacitic composition of approximately 63% $SiO_2$. In order to achieve the nearly 75% $SiO_2$ of the mature phase GRV, a second stage model was run, with the most mafic GRV dacite used as a middle composition and a pressure of one kbar. This is what produces the 'step' in the modelled trends.

Geochemically, the *Rhyolite-MELTs* model fits very well with the observed GRV data. The major element oxide trends are predominantly reproduced quite accurately (see Figure 14). The $P_2O_5$ trend is not shown here as *Rhyolite-MELTs* was not able to model the crystallisation of apatite correctly, so this was the one trend that did not fit the data. The $FeO_{(T)}$ content is a little low across the trend, while CaO and $TiO_2$ could be considered to be a bit high. While the $Al_2O_3$ trend is slightly too high at the beginning of the model, it aligns with the GRV data after about 58% $SiO_2$. The modelled NaO, $K_2O$, and MgO trends all align through the middle of the GRV data. Interestingly, the

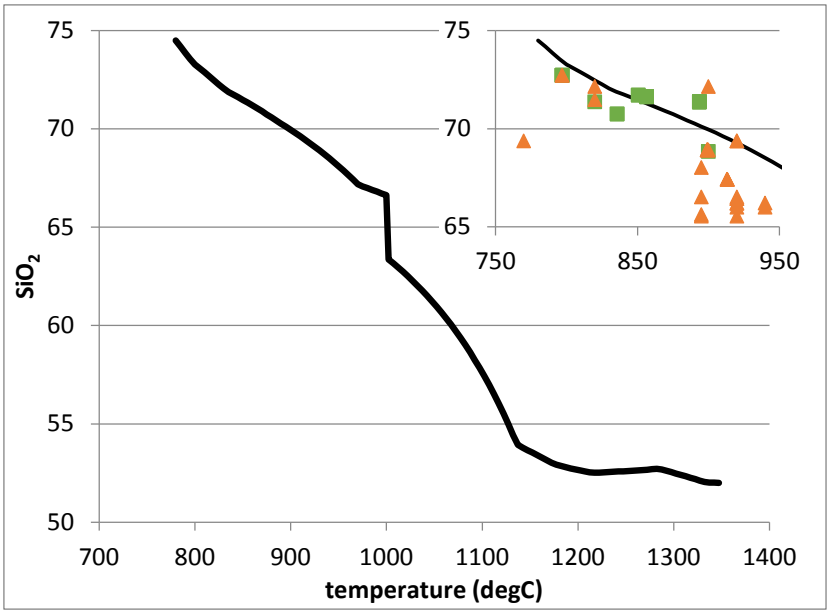


**Figure 13: wt. % $SiO_2$ vs. temperature of the GRV as modelled by Rhyolite-MELTs. Inset is a subset of the same graph with temperatures for the Eucarro and Yardea Dacites calculated by methods described by (Putirka 2008).**

core pyroxenites are all either clustered around the beginning of the *Rhyolite-MELTs* model trend or lie in direct line with it. This will be discussed later.

This modelling indicates that the most voluminous GRV, the Eucarro and Yardea Dacites, at around 65-72% $SiO_2$, would be the product of approximately 80% crystallisation (see Figure 12). The mature phase GRV would thus require about four times their mass as gabbroic and pyroxenitic crustal intrusives, the evidence for which is severely lacking. This also requires the volume of the primary melt to be significantly large, as these two units make up the greatest portion of the GRV but by this model reflect only a small volume of the total magma.

Using the thermometer and barometer calculation equations from Putirka (2008), mineral-specific data from microprobe analyses was used to make pressure and temperature estimates for a limited number of GRV rocks. Most of the calculations were based on minerals found in the Eucarro and Yardea Dacites. A subset of these calculations can be found in the inset of Figure 13, in comparison with the *Rhyolite-*

*MELTs* model. The returns from these calculations were consistent with those from the *Rhyolite-MELTs* modelling. The *Rhyolite-MELTs* model indicates crystallisation began at 1347$^0$C. The Yardea and Eucarro Dacites began crystallising at about 1000$^0$C and continued to crystallise through to about 840$^0$C. This is also indicated on Figure 13. The temperature returns from both the modelling and the calculations are largely consistent with the temperature range previously calculated by Agangi et al. (2012) for the mature phase GRV at around 900-1100$^0$C.

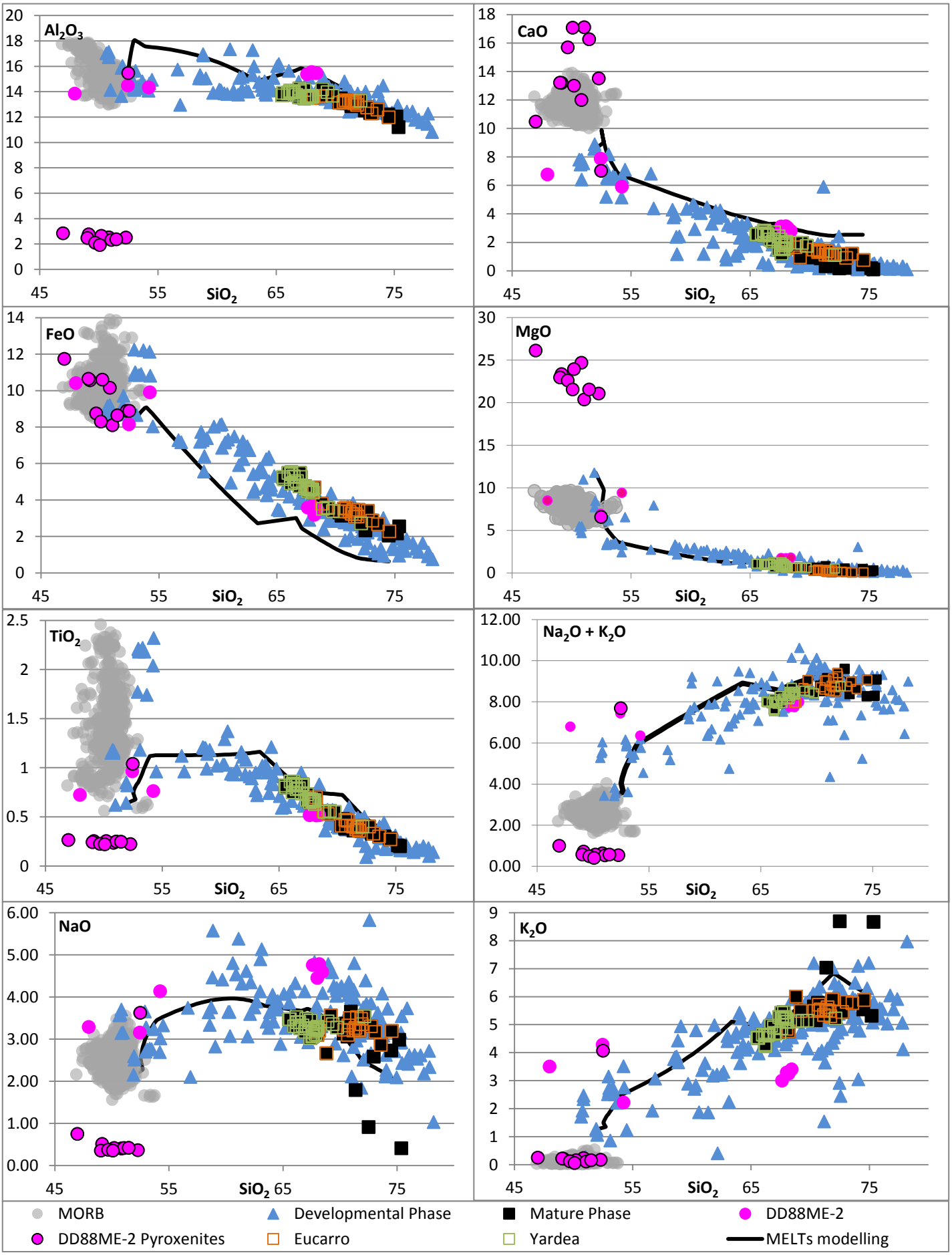


**Figure 14: Rhyolite-MELTs modelling compared with the variation of major element oxides vs. $SiO_2$ for the GRV (data from Stewart (1994)), samples from drillhole DD88ME-2, and MORB (data from Melson et al. (2002)).**

Temperatures from zircon saturation calculations are also consistent with these calculations, with a range of 840-940$^0$C (see Figure 15b) for the inflection point of the GRV samples. The inflection occurs at about 70% $SiO_2$ wt.%. This inflection point is where zircon becomes saturated in the magma with falling temperatures and increasing $SiO_2$. This is also the point where differentiation increases. At $SiO_2$ <70%, the magma is zircon under-saturated and magma T is greater than zircon saturation T. On the other side of this inflection point, zircon saturation temperature is greater than magma temperature, and zircon becomes saturated. In Figure 15c, a comparison is made between the zircon saturation temperatures and the calculated temperatures from the thermometers of Putirka (2008). It can be seen that most of the calculations fall around this inflection point.

The zircon saturation inflection point is also very similar to the inflection point in Nd versus $SiO_2$ (Figure 16). The Nd inflection point shows the change from Nd enrichment during fractionation to depletion. Again, this inflection occurs at around 70 wt.% $SiO_2$. These inflection points likely indicate an on-set of saturation of several accessory phases that take in Zr and well as REE, such as zircon, apatite, and allanite.

While the *Rhyolite-MELTs* model fits the major elements data for the GRV quite well, there is a significant amount of variation in the $\varepsilon_{Nd}$ values across the GRV that cannot be accounted for by pure fractional crystallisation. It is therefore concluded that there must have been some amount of assimilation of crust into the parental magma.

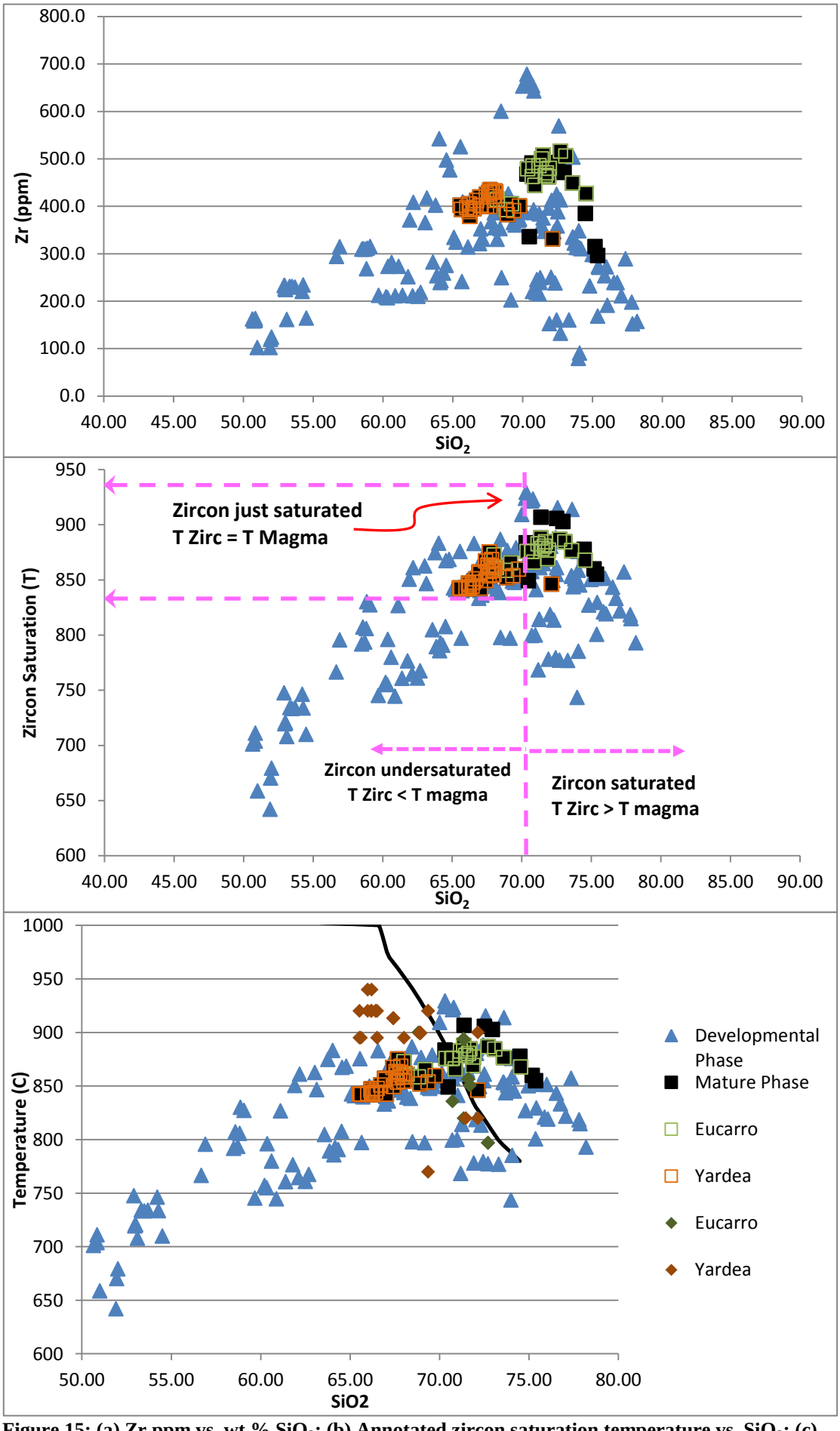


**Figure 15: (a) Zr ppm vs. wt.% $SiO_2$; (b) Annotated zircon saturation temperature vs. $SiO_2$; (c) Temperature (°C) vs. $SiO_2$ wt.%. This plot shows the zircon saturated temperature with the addition of the calculated temperatures for a series of Yardea and Eucarro samples and a portion of the *Rhyolite-MELTs* modelling**

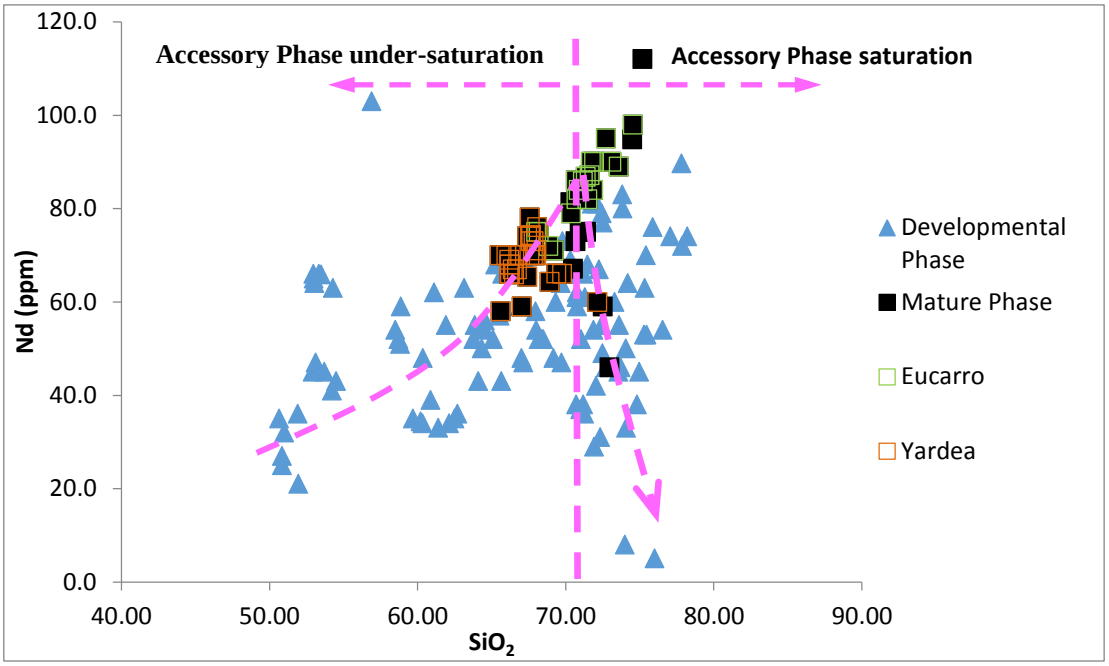


**Figure 16: annotated Nd (ppm) vs. $SiO_2$ wt. % graph with the inflection point labelled by the pink lines. To the left of the inflection point, accessory phase minerals are under-saturated. To the right, accessory phase minerals are saturated.**

## Combined AFC processes

While the Rhyolite-MELTs program shows that the variation from the most primitive GRV basalt to the most felsic GRV rhyolite can be modelled based on pure fractional crystallisation, there is significant variation in the $\varepsilon_{Nd}$ trends that indicates some level of crustal contamination must have occurred. The inflection point of the observed GRV Nd data informed the development of a two-stage AFC model. Two such models were made using different possible parent magma compositions. The first was based on a MORB-like parent and the second based on a contaminated mantle composition calculated from the most primitive GRV basalt. In both cases, the crustal contaminant is Gawler Craton Archean crust. The values for the crust were calculated as an average from data presented by Stewart (1994). The final models presented here are the end result of an essentially trial and error process, where certain values were varied. The key value was known as the r-value. This value quantified the rate of assimilation/ rate of

crystallisation, where an r-value of zero would represent pure fractional crystallisation. As an example, an r-value of 0.3 would mean that when the magma reaches 100% crystallisation, 30% of its final volume would have been from assimilation. This would then mean that a lower starting magma volume would be required to produce the final magma than for pure fractional crystallisation. In the case of the GRV, this would help to explain why the felsic material can be so voluminous in comparison to the mafic material.

*Option One – can the GRV result from fractionation of a MORB parent source with GC Archean crust contamination?*

Based on a two-stage model of coupled AFC processes, the Nd trend shown in Figure 17 was produced. This model started with a MORB-like parent composition. In the first stage, GC Archean crust was added with an r-value of 0.3. This produced the first half of the trend until the inflection point, where εNd is about -4.5. After this point, the r-value was changed to 0.25. This was able to produce a modelled $\varepsilon_{Nd}$ evolution that fit the GRV data;

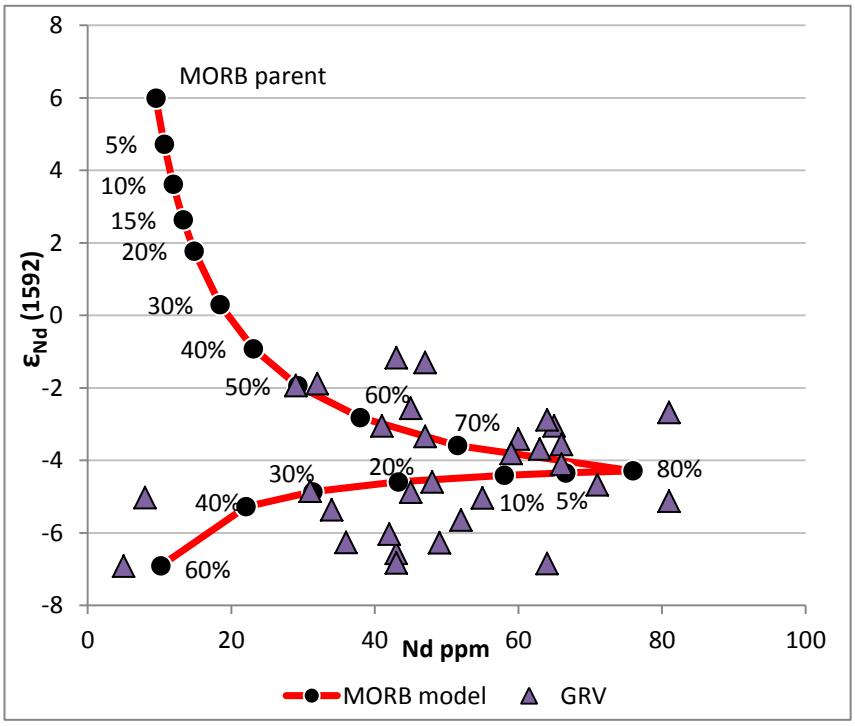


**Figure 17: Option One – a two-Stage AFC model with MORB parent. Percentages indicate the amount of crystallisation. The first stage was modelled with r=0.3 and the second stage with r=0.25. the model meets the observed data at 50% crystallisation.**

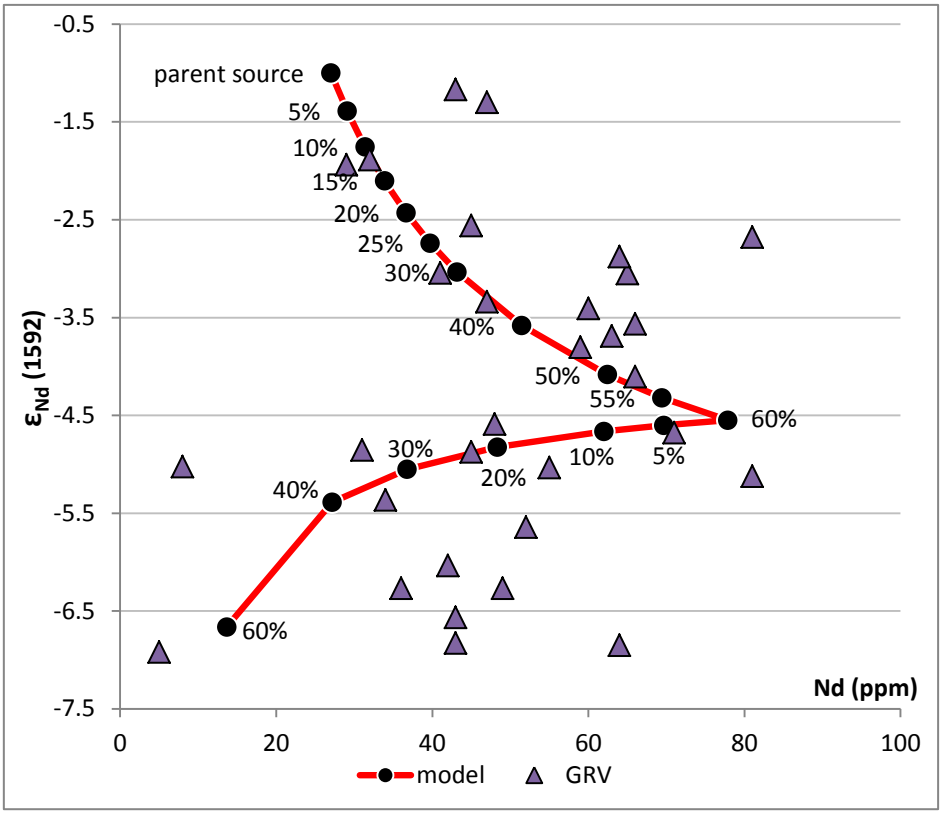


**Figure 18: Option Two – a two-stage AFC modelling with Contaminated Mantle source. Percentages are amounts of crystallisation. The first stage was modelled based on r=0.38 and the second stage with r =0.25. The model lines up with the observed GRV data at about 5% crystallisation.**

however, this magma required approximately 50% crystallisation before the model agreed with the GRV data. In addition, 80% of the total volume of magma would have to crystallise before the inflection point was reached.

*Option Two – can the GRV result from fractionation of a Contaminated Mantle parent source with GC Archean crust contamination?*

Again using a two-stage model of coupled AFC processes, the Nd trend in Figure 18 was produced. This time, however, the starting parent composition was a contaminated mantle composition based on the most primitive GRV basalts. This primary magma was back-fractionated from the most primitive GRV basalt using the methods of Lee et al. (2009). It is of interest that these methods did not change the composition of the GRV

basalt very much in order to reach the most primitive parent composition. Compared to average MORB composition, this melt composition is high in $SiO_2$, very high in MgO, Cr and Ni, and low in CaO, $Na_2O$, total FeO and $TiO_2$. This composition indicates that the source of the GRV melt was most likely a depleted refractory mantle as far as the major elements are concerned. The high $SiO_2$ and very high $Cr_2O_3$ indicate an orthopyroxene peridotite source, while the low CaO and $Na_2O$ suggest the source was deficient in clinopyroxene. This is a harzburgite source, which has been demonstrated to dominate the sub-continental lithospheric mantle beneath Archean cratons such as the Gawler Craton (Griffin et al. 2003).

The crustal component used as the assimilant was the same as the previous model. In the first stage, GC Archean crust was added with an r-value of 0.38. In the second stage, after the inflection point in the Nd data, the r-value was 0.25. This model produces a good match for the GRV data. About 5% crystallisation is required to reach the GRV data trend. Like the MORB model, this model also requires a large amount of crystallisation to reach the inflection point – approximately 60%.

While both models were able to mimic the trends of the GRV reasonably well, the MORB-like parent model required a very large amount of crystallisation to reach the GRV data. This would therefore suggest that the volume of the initial magma chamber would have been at least twice the volume of the extruded GRV. This seems unlikely. On the other hand, the contaminated mantle source requires less crystallisation before the modelled trends match up with the actual data. This reduces the size of the initial magma chamber in comparison to the MORB-like parent, however the model still requires a great deal of crystallisation to reach the inflection point. In either case, the magma chamber must be very large to account for the $\varepsilon_{Nd}$ trend by this method.

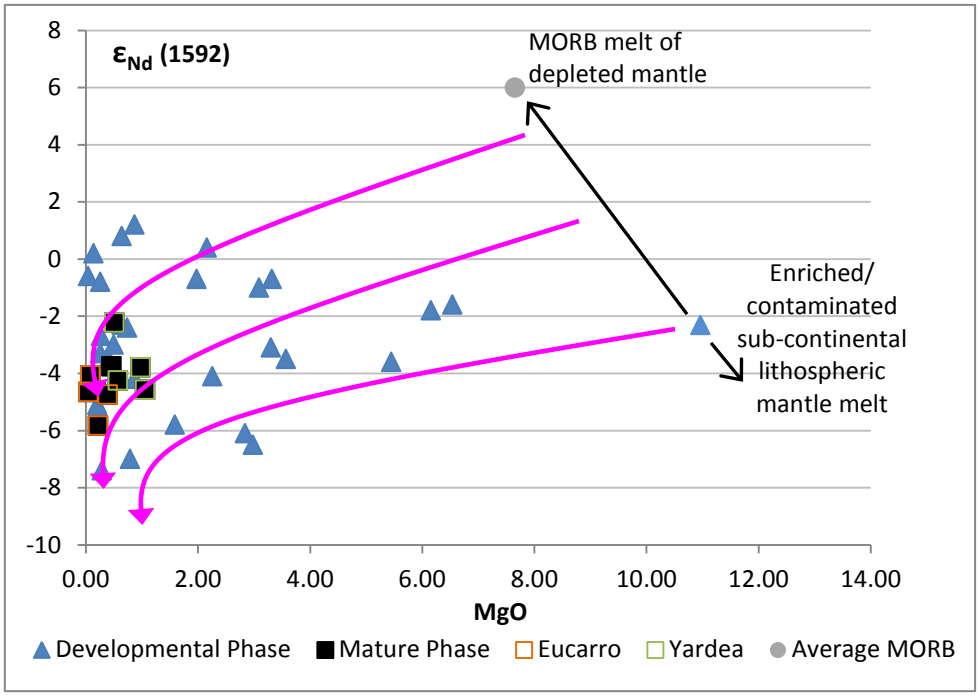


**Figure 19: annotated $\varepsilon_{Nd}$ (1592) vs. MgO wt.% showing multiple trends in AFC evolution of the GRV, with average MORB (data from Melson et al. (2002)) representing one possible end-member starting composition.**

## Multiple trends (?)

Although only one AFC trend has been calculated for the entire GRV in these models, it is likely that multiple AFC trends could be calculated. As can be seen in Figure 19, the $\varepsilon_{Nd}$ values appear to define several similar trends. The black arrow proposes two possible end-member starting compositions: an average MORB composition and the most primitive GRV basalt. In this case, the arrow extends beyond the most primitive GRV basalt as it is likely that the end-member is somewhere beyond this sample. Three trends have been defined, with an asthenosphere (e.g. MORB) trend in the uppermost $\varepsilon_{Nd}$ range. This trend may be more heavily influenced by asthenospheric melt than the lower $\varepsilon_{Nd}$ range trends, which may be more closely linked to a contaminated mantle source.

## Core samples

The origin of the core rocks is still not one hundred percent certain and more data needs to be obtained to make a better assessment. Geographically, the drillhole is positioned relatively close to where known outcrop of the GRV exists (see Figure 1) and is certainly in the region where the GRV are predicted to extend beneath younger sediments (McPhie et al.). While based on the major element chemistry they seem to fit the GRV data reasonably well, some of the minerals in thin section appear to be too fresh to be of GRV age. In addition, the succession of rocks in the core is complicated and the relationships are not well understood due to the limited window into the subsurface that drillholes provide. In particular, questions remain about how the pyroxenites came to be interlayered with the extrusives and more felsic compositions. One contact between an andesite and a pyroxenite appears to be gradual, suggesting the pyroxenite may have been brought up from the magma chamber by the andesite as a crystal slurry when it extruded. The more intermediate to felsic compositions from the core rocks plot similarly to the GRV in the Harker diagrams (see Figure 3). In particular, the dacites seem to have major element compositions close to the Yardea Dacite. The biggest difference is in the $K_2O$ plot, although this could be a result of K being mobilised by alteration processes. The core shows evidence of various forms of alteration throughout.

Largely, the core rocks have very similar major element trends. However, the PMN trace element signatures vary significantly from the GRV patterns, particularly in the HFSE. There is a certain amount of variation within the known GRV though, so this does not entirely exclude these rocks as being classified as part of the GRV. Additionally, the pyroxenites plot around the beginning of the trends, where it would be

expected that cumulative residues from the GRV would be located, geochemically. The compositions of the pyroxenites are very similar to those calculated in the early stages of the *Rhyolite-MELTs* model. As such, conclusions can only be tentatively drawn when relating the core rocks to the GRV.

Of particular interest for further study would be the $\varepsilon_{Nd}$ values. Knowing these would help compare the core rocks with the GRV both in terms of age and in compositional heritage. In addition, microprobe analysis of the thin sections would help to determine the nature of some of the more unusual minerals, such as the apparently and unexpectedly fresh olivines.

## The volume problem

The mature phase GRV have an approximate minimum volume of 4,000 $km^3$ (Stewart 1994). The Yardea Dacite is at least 3000 $km^3$ (Creaser and White 1991) and the Eucarro Dacite is at least 675 $km^3$ (Allen and McPhie 2002). These volumes appear to be based on the mapped extent of the units at the surface and the known thickness extent. Estimates quoted earlier included shows in drillholes, but these are relatively sparsely located and so do not define the outer limits with as much certainty as the outcrop extent.

Based on *the Rhyolite-MELTs* modelling, the magma source would have had to reach about 80% crystallisation before the composition of the mature phase GRV would have been reached. This means that the volume of the magma must have been at least four times the volume of the mature phase volcanics. As a minimum, this means that there should be about 16,000 $km^3$ of material that is more mafic to intermediate in composition. This estimate is based on pure fractional crystallisation, however it has been shown that a coupled AFC process was most likely acting on the GRV magma

chamber in order for the observed $\varepsilon_{Nd}$ variation to be achieved. This would reduce the volume of the initial magma required to produce the mature phase GRV as some of the volume would be from addition of contaminant to the primary melt. The rate of assimilation over the rate of crystallisation (r-value) used to produce the AFC model from a contaminated mantle source with GC crustal contamination determines the final volume of the required magma source. The model shows that only low r-values are required to achieve the $\varepsilon_{Nd}$ variation observed in the GRV. This means that the calculated 16,000 $km^3$ would be an overestimate for the AFC model, but not by very much. In addition, the GRV are old and significantly weathered, so the calculated volume of the mature phase GRV is almost certainly lower than the original volume.

## CONCLUSIONS

Based on the work of Lee et al. (2009) the potential primary melt of the Gawler Range Volcanics has been calculated. This composition required very little back-fractionation from the most primitive GRV basalt to be obtained. The composition indicates a refractory harzburgite source. The calculated pressure that accompanies the compositional back-fractionation calculations indicates a shallow origin for the LPT basalts. This pressure indicates a depth of around 50 km, which is well inside the SCLM. However, the temperature calculations indicate that this region was significantly heated from the usual expected $850^0$C to greater than $1360^0$C. Two possible mechanisms of introducing this heat are a mantle plume or delamination of the lithospheric mantle (Pysklywec et al. 2010).

While the most primitive basalts in the GRV have this refractory mantle harzburgite source composition for the major elements, the trace elements and $\varepsilon_{Nd}$ values are more crust-like. This indicates that the GRV melt had crustal geochemical features before any

fractionation began. This suggests that the refractory mantle source was already re-enriched by a contaminant of crustal origin. As discussed by Stewart (1994), sometime before the Gawler Range volcanism the SCLM below the Gawler Craton was modified to become enriched in REE and LILE but not HFSE. This enrichment may be related to an Archean event (Stewart 1994).

The AFC modelling based on the variation in $\varepsilon_{Nd}$ values for the GRV indicates that this refractory mantle source was contaminated by crustal material. The model suggests that around 5% crustal contamination from the Gawler Craton into a depleted mantle source would be required in order to produce the $\varepsilon_{Nd}$ values observed for the GRV. The PMN trace element diagram also indicates that about 15% partial melting of this source is required to achieve the observed trace element patterns. It also indicates that about 13% garnet was present in the source composition. Based on the inflection point in the $\varepsilon_{Nd}$ trend, a two-stage AFC model of magma chamber evolution is required and has been calculated. However, the $\varepsilon_{Nd}$ values also indicate that multiple fractionation trends are more likely responsible for the GRV than one single trend.

The *Rhyolite-MELTs* modelling indicates that the entire GRV suite can be achieved in one fractionation trend. However, the most voluminous mature phase GRV compositions are not reached until about 80% crystallisation of the magma in this model. This would indicate that the mafic and intermediate GRV compositions should account for five times the volume of the felsic GRV. With an estimated volume of 4,000 $km^3$ for the mature phase GRV, this requires at least 16,000 $km^3$ volume for the parental basalt, most of which must remain in the lower to mid crust. This is a maximum estimate, however, as the AFC process that have been demonstrated to have been acting

on the GRV melt mean that a certain amount of crustal material was assimilated into this parent basalt, which lowers the required initial volume.

That the developmental phase and mature phase GRV can be linked by a single fractionation trend according to the *Rhyolite-MELTs* model adds weight to the interpretation that the GRV are likely the results of varying amounts of mixing between to end-member sources. Given the multiple trends observed in the $\varepsilon_{Nd}$ data, it is possible that one end-member is the modelled re-enriched harzburgite source and the other is more similar to an asthenospheric mantle source such as MORB.

Further work could be done to expand the number of samples taken from the GRV, possibly by adding data from more recent studies to generate one more comprehensive database. This could help to reinforce the trends and to add more certainty to their interpretation. Given the range in $\varepsilon_{Nd}$ values, the collection/ calculation of more Nd data would be beneficial to better constrain these interpreted trends. This would further allow for assessment of the AFC processes that produced the GRV as separate trends based on the $\varepsilon_{Nd}$ trends. Additional analysis of the core rock samples would also help to either classify or declassify these rocks as GRV with more definitive certainty. This would then allow for more interpretation of the relationship between these rocks with the wider GRV, if they were proven to be related.

## ACKNOWLEDGMENTS

I would like to thank my supervisor, Professor John Foden, for his advice, direction, support, and for imparting some of his extensive knowledge. For their assistance in preparing my core samples for geochemical analysis, David Bruce and John Stanley also deserve many thanks. I would also like to express gratitude to the staff of Adelaide Microscopy, especially Aoife McFadden, Ken Neubauer and Dr. Ben Wade, for their guidance and support. I would also like to thank Claire Wade from the Department of State Development for her assistance, advice and her attempt at guiding me through my field work (for the few hours we were in the field before getting rained out). Finally, I

would like to express my enormous gratitude for Dr. Katie Howard, who offered plenty of support throughout the year – both moral and academic.

## REFERENCES

AGANGI A. 2011 Magmatic and volcanic evolution of a silicic large igneous province (SLIP): the Gawler Range Volcanics and Hiltaba Suite, South Australia. pp. 203. University of Tasmania.
AGANGI A., KAMENETSKY V. S. & MCPHIE J. 2010. The role of flourine in the concentration and transport of lithophile trace elements in felsic: Insights from the Gawler Range Volcanics, South Australia. *Chemical Geology,* **vol. 273**, pp. 314-325.
AGANGI A., KAMENETSKY V. S. & MCPHIE J. 2012. Evolution and emplacement of high fluorine rhyolites in the Mesoproterozoic Gawler silicic large igneous province, South Australia. *Precambrian Research,* **vol. 208–211**, no. 0, pp. 124-144.
ALLEN S., MCPHIE J., SIMPSON C., KAMENETSKY V. S., CHAMBEFORT I., AGANGI A., BATH A., GARNER A. & MORROW N. 2009 A Mesoproterozoic silicic LIP in South Australia: the Gawler Range Volcanics and Hiltaba Suite. Large Igneous Provinces Comission.
ALLEN S. R. & MCPHIE J. 2002. The Eucarro Rhyolite, Gawler Range Volcanics, South Australia: A >675 $km^3$, compositionally zoned lava of Mesoproterozoic age. *Geological Society of America,* **vol. 114**, no. 12, pp. 1592-1609.
ALLEN S. R., MCPHIE J., FERRIS G. & SIMPSON C. 2008. Evolution and architecture of a large felsic Igneous Province in western Laurentia: The 1.6 Ga Gawler Range Volcanics, South Australia. *Journal of Volcanology and Geothermal Research,* **vol. 172**, no. 2008, pp. 132-147.
ALLEN S. R., SIMPSON C. J., MCPHIE J. & DALY S. J. 2003. Stratigraphy, distribution and geochemistry of widespread felsic volcanic units in the Mesoproterozoic Gawler Range Volcanics, South Australia. *Australian Journal of Earth Sciences,* **vol. 50**, pp. 97-112.
ARNDT N. T., COLTICE N., HELMSTAEDT H. & GREGOIRE M. 2009. Origin of Archean subcontinental lithospheric mantle: Some petrological constraints. *Lithos,* **vol. 109**, no. 1–2, pp. 61-71.
BRYAN S. E., EWART A., STEPHENS C. J., PARIANOS J. & DOWNES P. J. 2000. The Whitsunday Volcanic Province, Central Queensland, Australia: lithological and stratigraphic investigations of a silicic-dominated large igneous province. *Journal of Volcanology and Geothermal Research,* **vol. 99**, no. 1–4, pp. 55-78.
COLLINS W. J., BEAMS S. D., WHITE A. J. R. & CHAPPELL B. W. 1982. Nature and origin of A-type granites with particular reference to southeastern Australia. *Contributions to Mineralogy and Petrology,* **vol. 80**, no. 2, pp. 189-200.
CREASER R. A. & WHITE A. J. R. 1991. Yardea Dacite—Large-volume, high-temperature felsic volcanism from the Middle Poterozoic of South Australia. *Geology,* **vol. 19**, pp. 48-51.
DEPAOLO D. J. 1981. Trace element and isotopic effects of combined wallrock assimilation and fractional crystallization. *Earth and Planetary Science Letters,* **vol. 53**, no. 2, pp. 189-202.
FANNING C. M., FLINT R. B., PARKER A. J., LUDWIG K. R. & BLISSETT A. H. 1988. Refined Proterozoic evolution of the Gawler Craton, South Australia, through U-Pb zircon geochronology. *Precambrian Research,* **vol. 40–41**, no. 0, pp. 363-386.
FRANCIS D. 2003. Cratonic mantle roots, remnants of a more chondritic Archean mantle? *Lithos,* **vol. 71**, no. 2–4, pp. 135-152.
FROST B. R., BARNES C. G., COLLINS W. J., ARCULUS R. J., ELLIS D. J. & FROST C. D. 2001. A Geochemical Classification for Granitic Rocks. *Journal of Petrology,* **vol. 42**, no. 11, pp. 2033-2048.
GILES C. W. 1988. Petrogenesis of the Proterozoic Gawler Range Volcanics, South Australia. *Precambrian Research,* **vol. 40–41**, no. 0, pp. 407-427.
GREENLAND L. P. 1970. An equations for trace element distrinution during magmatic crystallization. *The American Mineralogist,* **vol. 55**, no. March-April, pp. 455-465.
GRIFFIN W. L., O'REILLY S. Y., ABE N., AULBACH S., DAVIES R. M., PEARSON N. J., DOYLE B. J. & KIVI K. 2003. The origin and evolution of Archean lithospheric mantle. *Precambrian Research,* **vol. 127**, no. 1–3, pp. 19-41.
GUALDA G. A. R., GHIORSO M. S., LEMONS R. V. & CARLEY T. L. 2012. Rhyolite-MELTS: a Modified Calibration of MELTS Optimized for Silica-rich, Fluid-bearing Magmatic Systems. *Journal of Petrology,* **vol. 53**, no. 5, pp. 875-890.

JENNER F. E. & O'NEILL H. S. C. 2012. Analysis of 60 elements in 616 ocean floor basaltic glasses. *Geochemistry, Geophysics, Geosystems,* **vol. 13**, no. 2, p. Q02005.
KAMENETSKY V. S., MORROW N. & MCPHIE J. 2000. Origin of high-Si dacite from rhyolitic melt: evidence from melt inclusions in mingled lavas of the 1.6 Ga Gawler Range Volcanics, South Australia. *Mineralogy and Petrology,* **vol. 69**, pp. 183-195.
LE BAS M. J., LE MAITRE R. W., STRECKEISEN A., ZANETTIN B. & ROCKS) O. B. O. T. I. S. O. T. S. O. I. 1986. A Chemical Classification of Volcanic Rocks Based on the Total Alkali-Silica Diagram. *Journal of Petrology,* **vol. 27**, no. 3, pp. 745-750.
LEE C.-T. A., LUFFI P., PLANK T., DALTON H. & LEEMAN W. P. 2009. Constraints on the depths and temperatures of basaltic magma generation on Earth and other terrestrial planets using new thermobarometers for mafic magmas. *Earth and Planetary Science Letters,* **vol. 279**, no. 1–2, pp. 20-33.
MCPHIE J., DELLAPASQUA F., ALLEN S. R. & LACKIE M. A. 2008. Extreme effusive eruptions: Palaeoflow data on an extensive felsic lava in the Mesoproterozoic Gawler Range Volcanics. *Journal of Volcanology and Geothermal Research,* **vol. 172**, no. 1–2, pp. 148-161.
MELSON W. G., O'HEARN T. & JAROSEWICH E. 2002. A data brief on the Smithsonian Abyssal Volcanic Glass Data File. *Geochemistry, Geophysics, Geosystems,* **vol. 3**, no. 4, pp. 1-11.
NIMIS P. 1999. Clinopyroxene geobarometry of magmatic rocks. Part 2. Structural geobarometers for basic to acid, tholeiitic and mildly alkaline magmatic systems. *Contributions to Mineralogy and Petrology,* **vol. 135**, no. 1, pp. 62-74.
PUTIRKA K. D. 2008 Thermometers and Barometers for Volcanic Systems. In PUTIRKA K. D. & TEPLEY III F. J. eds. Minerals, Inclusions and Volcanic Processes. pp. 61-120. Virginia, U.S.A: Mineralogical Society of America.
PYSKLYWEC R. N., GOGUS O., PERCIVAL J., CRUDEN A. R. & BEAUMONT C. 2010. Insights from geodynamical modeling on possible fates of continental mantle lithosphere: collision, removal, and overturn. *Canadian Journal of Earth Sciences,* **vol. 47**, no. 4, pp. 541-563.
ROLLINSON H. R. 1993 Using Geochemical Data: Evaluation, Presentation, Interpretation. Longman Group UK Limited, England.
SHAW D. M. 1970. Trace element fractionation during anatexis. *Geochimica et Cosmochimica Acta,* **vol. 34**, no. 2, pp. 237-243.
STEWART K. P. 1994 High temperaure felsic volcanism and the role of mantle magmas in Proterozoic crustal growth: The Gawler Range Volcanic Province. Department of Geology and Geophysics. pp. 334. South Australia: The University of Adelaide.
SUN S.-S. & MCDONOUGH W. F. 1989. Chemical and isotopic systematics of oceanic basalts: implications for mantle composition and processes. *Geological Society, London, Special Publications,* **vol. 42**, pp. 313-345.
WADE C. E., REID A. J., WINGATE M. T. D., JAGODZINSKI E. A. & BAROVICH K. 2012. Geochemistry and geochronology of the c. 1585 Ma Benagerie Volcanic Suite, southern Australia: Relationship to the Gawler Range Volcanics and implications for the petrogenesis of a Mesoproterozoic silicic large igneous province. *Precambrian Research,* **vol. 206–207**, no. 0, pp. 17-35.
WATSON E. B. 1979. Zircon saturation in felsic liquids: Experimental results and applications to trace element geochemistry. *Contributions to Mineralogy and Petrology,* **vol. 70**, no. 4, pp. 407-419.
WHALEN J., CURRIE K. & CHAPPELL B. 1987. A-type granites: geochemical characteristics, discrimination and petrogenesis. *Contributions to Mineralogy and Petrology,* vol. 95, no. 4, pp. 407-419.

## APPENDIX A: TABLE OF CALCULATED P/T DATA

| | Method: | Plag-Melt | Kspar-Melt | Olivine-liq | Olivine-liq | Hbl-Plag | | Mean T | | CPXBar | |
|---|---|---|---|---|---|---|---|---|---|---|---|
| | Author: | Putirka | Putirka | Putirka | Sisson & Grove (1992) | Blundy and Holland | | | | Nimis and Taylor | |
| | | Eqn (24a) | Eqn (24b) | Eqn. (2) | Eqn. 2 | | | | | | |
| Rock sample | Measurement: | T(C ) | T(C ) | T(C ) | T(C ) | T (C) | P | | | P (kbar) | at T |
| Eu7 | | 903 | | | | | | 894 | | 1.4 | 820 |
| Eu7 | | 893 | | | | | | 894 | | | |
| Eu7 | | 910 | | | | | | 894 | | | |
| Eu7 | | | 877 | | | | | 894 | | | |
| Eu7 | | | 893 | | | | | 894 | | | |
| Eu7 | | | 887 | | | | | 894 | | | |
| Eu21 | 860 | | | 825 | 856 | | | 851 | | | |
| Eu21 | 861 | | | | | | | 851 | | | |
| Eu2 | 856 | | | | | 825 | 1 | 836 | | | |
| Eu2 | 848 | | | | | 814 | 2 | 836 | | | |
| Eu5 | 857 | 891 | | | | | | 857 | | | |
| Eu5 | 849 | 894 | | | | | | 857 | | | |
| Eu5 | | 878 | | | | | | 857 | | | |
| Eu5 | | 891 | | | | 777 | 2 | 857 | | | |
| Eu5 | | 894 | | | | | | 857 | | | |
| Eu5 | | 878 | | | | | | 857 | | | |
| Y31 | 915 | | | | | 756 | 1 | 913 | | 1.1 | 913 |
| Y31 | 914 | | | | | | | 913 | | | |
| Y31 | 911 | | | | | | | 913 | | | |

| | | | | | | | | | | | |
|---|---|---|---|---|---|---|---|---|---|---|---|
| WA4 | 902 | | | | | | | 899 | | 1.9 | 900 |
| WA4 | 897 | | | | | | | 899 | | | |
| WA4 | 900 | | | | | | | 899 | | | |
| WA3 | | 755 | | | | 784 | 1 | 770 | | 2.4 | 920 |
| Eu20 | | | 766 | 802 | | | | 797 | | 1.7 | 797 |
| Eu20 | | | 793 | 826 | | | | 797 | | 0.9 | 797 |
| A2 | | | | | | 776 | 2 | 776 | | | |
| A2 | | | | | | 779 | 1 | 779 | | | |
| Y32 | | | | | | | | | | 1.9 | 920 |
| Y45 | | | | | | | | | | 1.6 | 940 |
| Y47 | | | | | | | | | | 1.2 | 940 |
| Y49 | | | | | | | | | | 1.6 | 920 |
| Eu10 | | | | | | | | | | 0.2 | 900 |
| 849-36 | | | | | | | | | | 0.0 | 820 |
| Y4 | | | | | | | | | | 2.1 | 920 |
| Y4 | | | | | | | | | | 1.0 | 895 |
| Y5 | | | | | | | | | | 1.8 | 895 |
| Y12 | | | | | | | | | | 0.9 | 895 |
| Y19 | | | | | | | | | | 0.7 | 900 |
| Y19 | | | | | | | | | | 1.1 | 913 |
| WA3 | | | | | | | | | | 1.4 | 920 |
| WA4 | | | | | | | | | | 0.7 | 899 |
| Y32 | | | | | | | | | | 1.6 | 895 |
| Y45 | | | | | | | | | | 1.9 | 920 |
| Y46 | | | | | | | | | | 1.2 | 920 |
| Y47 | | | | | | | | | | 1.7 | 920 |
| Y49 | | | | | | | | | | 1.6 | 920 |

## APPENDIX B: CORE LOG DETAILS

| Depth (m) (from) | Depth (m) (to) | Geology notes (adapted from Drill Hole Log DD88ME-2 by Palmer 1988) | Sample number | Sample depth (m) (from) | Sample depth (m) (to) | Thin section notes |
|---|---|---|---|---|---|---|
| 0 | 69 | COVER SEQUENCE - interlayered sandstones and claystones | | | | |
| 69 | 72 | WEATHERED BASEMENT/ SANDSTONE | | | | |
| 72 | 74.5 | PORPHYRITIC DACITE/ RHYODACITE – brown to grey weathered porphyritic intermediate volcanic consisting of euhedral phenocrysts of plagioclase (25%) and subordinate k-spar (15%) with fine laths of hornblende and biotite distributed throughout. Fine crystalline quartz dominated groundmass. Core is broken and there are numerous crosscutting chlorite-serpentinite veinlets with minor iron oxide and micro-brecciation/ fracturing. | 2067545 | 73.2 | 73.3 | |
| | | 74.5-94.9 m <u>PYROXENITE WITH INTERLAYERED DACITE/ RHYODACITE AND DISCORDANT PEGMATITES AND RARE DOLERITE</u><br>rock weathered to 81 m. core very broken and fragmented, obscuring structure. | | | | |
| 74.5 | 75.55 | PYROXENITE – dark green to grey, weathered, massive medium crystalline pyroxenite comprising of altered plagioclase and olivine (40%), euhedral amphibole (25%), disseminated magnetite (10-15%) and scattered phenocrysts of euhedral biotite (10-15%). Possibly up to 10% pyroxene. Trace disseminated pyrite and chalcopyrite. Core broken. | | | | |
| 75.55 | 76.3 | PORPHYRITIC DACITE – brown to grey dacite (as for 72-74.5 m) with k-spar-quartz (biotite) pegmatite at 76.4-76.5 m and chlorite and iron oxides lined fractures. Core broken. | 2067546 | 77.05 | 77.15 | |
| 76.3 | 84.12 | PYROXENITE – dark green to grey weathered massive medium | | | | |

| Depth (m) (from) | Depth (m) (to) | Geology notes (adapted from Drill Hole Log DD88ME-2 by Palmer 1988) | Sample number | Sample depth (m) (from) | Sample depth (m) (to) | Thin section notes |
|---|---|---|---|---|---|---|
| | | crystalline diorite comprising plagioclase (40%) and an interlocking mass of euhedral amphibole (25-30%), magnetite (10-15%), possibly pyroxene (5-10%) and biotite (10-15%) minor irregular quartz and calcite veinlets. Trace pyrite and chalcopyrite disseminated through rock. Discordant. K-spar-quartz-amphibole pegmatite from 81-81.3 | | | | |
| 84.12 | 84.8 | RHYODACITE – possibly discordant, comprising medium crystalline phenocrysts of plagioclase (25%) and k-spar (45%) which may be rotated (flow banding?) and subordinate quartz (20%). Some vesicles and amygdales. Minor amphibole and biotite. Well orientated chlorite between felspathic phenocrysts. Core loss between 84.35-84.8 m. | | | | |
| 84.8 | 85.28 | DOLERITE (?) – weathered discordant plagioclase-amphibole-k-spar-biotite dolerite, rock very friable | | | | |
| 85.28 | 87 | PYROXENITE – as for 76.5-84.12 m with thin (1-2 mm) siderite and quartz veinlets. Trace pyrite and chalcopyrite with veins. Minor clay coatings on some fracture surfaces. | 2067547 | 85.5 | 85.6 | -Large ex-olivines<br>-intercumulate mica? (pleochroic brownish) |
| 87 | 87.3 | PEGMATITE – quartz-k-spar-plagioclase-(biotite-chlorite) pegmatite. Medium to coarse crystalline, frequently fractured. | | | | |
| 87.3 | 88.45 | PYROXENITE – as for 85.28-87 m. trace pyrite and chalcopyrite | | | | |
| 88.45 | 88.9 | PEGMATITE – very coarsely crystalline, quartz (80%), k-spar (15%) and biotite (5%). Trace chlorite. Discordant with lower boundary | | | | |
| 88.9 | 89.7 | PYROXENITE – as for 85.28-87 m | | | | |
| 89.7 | 90 | Core loss | | | | |

| Depth (m) (from) | Depth (m) (to) | Geology notes (adapted from Drill Hole Log DD88ME-2 by Palmer 1988) | Sample number | Sample depth (m) (from) | Sample depth (m) (to) | Thin section notes |
|---|---|---|---|---|---|---|
| 90 | 91 | PEGMATITE – as for 87-87.3 m | | | | |
| 91 | 94.9 | PYROXENITE – as for 74.5-75.5 m, with discordant quartz vein at 94.2 m and from 94.4 m chloritic/ serpentinitic alteration of plagioclase and olivine within pyroxenite | | | | |
| | | 94.9-112.88 m <u>INTERLAYERED ULTRAMAFICS AND BASALT WITH DISCORDANT PEGMATITE BANDS</u><br>series of interlayered basic volcanics with discordant pegmatite bands. The basic volcanics are altered to hornblendites near the pegmatite bands. Rock very fractured and broken with quartz plagioclase veining and minor siderite veinlets | | | | |
| 94.9 | 95.45 | HORNBLENDITE WITH PEGMATITE – dark to light green, medium to coarse crystalline massive amphibole, altered rock, comprising euhedral amphibole (25%) with fine grained altered plagioclase. This appears to be an alteration halo to small discordant irregular k-spar-quartz pegmatite bands (contacts at 97.05-97.14, 95.27-95.3, and 94.45-95.5 m). Minor siderite and quartz veining with traces pyrite. | | | | |
| 95.45 | 95.8 | PYROXENITE – as for 76.5-84.12 | | | | |
| 95.8 | 97.4 | VESICULAR/ AMYGDALOIDAL BASALT – dark green-grey massive fine-grained rock with groundmass of mafic minerals and plagioclase. Irregularly scattered vesicles (1-3 mm) in diameter, which may be quartz or carbonate filled. Trace pyrite and chalcopyrite (97.1 m). Minor irregular quartz veining. Trace pyrite and chalcopyrite on fracture planes. | 2067548 | 97.05 | 97.15 | -crystal digestion (quartz lumps, scalloped edges indicate not veining; evidence of AFC – basalt digesting crust)<br>-unusually fresh phenocrysts of pyroxene |
| 97.4 | 98.8 | PYROXENITE – as for 76.5-84.12 m, with moderate quartz/ carbonate (?) veining (carbonate does not react with acid). | | | | |

| Depth (m) (from) | Depth (m) (to) | Geology notes (adapted from Drill Hole Log DD88ME-2 by Palmer 1988) | Sample number | Sample depth (m) (from) | Sample depth (m) (to) | Thin section notes |
|---|---|---|---|---|---|---|
| | | Small pegmatite band from 98.3-98.4 m | | | | |
| 98.8 | 99.2 | PEGMATITE – as above | | | | |
| 99.2 | 99.68 | PYROXENITE – as above with thin pyrite veins and minor carbonate at 99.5 m | | | | |
| 99.68 | 99.86 | HORNBLENDITE – similar to 94.9-95.45 m, with k-spar (20%) forming medium sized grains in ground mass with amphibole (50%), biotite (15%) and minor plag (<5%). Minor chalcopyrite as fine disseminated grains. Lower contact interpreted as alteration contact to pegmatite below | 2067549 | 99.8 | 99.9 | -phenocrysts of mica (probably phlogopite)<br>-olivine (green smudges in XPL, likely broken down, easier to see in PPL)<br>-clinopyroxene (bright blue in XPL, equant crystals)<br>-lamprophyre<br>-Mg ad K rich<br>-delicately preserved texture |
| 99.86 | 100.23 | PEGMATITE – k-spar-quartz-biotite rock with thin amphibolitic margins | | | | |
| 100.23 | 100.85 | PYROXENITE – weakly amphibolitic altered with carbonate veining | | | | |
| 100.85 | 101.63 | HORNBLENDITE – as for 99.68-99.86 m | | | | |
| 101.63 | 106.45 | PEGMATITE – coarse crystalline felsic pegmatite consisting of quartz (35%), k-spar (25%), microcline? (35%), and minor biotite (5%), with minor amphibolitic xenoliths and carbonate/clay veining. Minor amphibole-biotite-k-spar veining | | | | |
| 106.45 | 112.88 | PYROXENITE – dark green to grey, massive to very weakly foliated, medium crystalline pyroxenite comprising plag (35-40%), pyroxene (25-30%), magnetite (10-15%) and biotite (10- | 2067550 | 106.5 | 106.6 | |

| Depth (m) (from) | Depth (m) (to) | Geology notes (adapted from Drill Hole Log DD88ME-2 by Palmer 1988) | Sample number | Sample depth (m) (from) | Sample depth (m) (to) | Thin section notes |
|---|---|---|---|---|---|---|
| | | 15%). Trace disseminated pyrite and rare chalcopyrite. Abundant carbonate and quartz veining (some with clay) at irregular orientations and serpentine | | | | |
| 112.88 | 118.47 | PORPHYRITIC ANDESITE WITH MINOR DISCORDANT DOLERITE BANDS – dark grey to grey-green porphyritic andesite comprising of subhedral plagioclase phenocrysts (up to 2 mm; 30%), weakly orientated biotite laths (25%) and minor hornblende (5-10%). Core now competent | | | | |
| 118.47 | 119.05 | HORNBLENDITE – as for 94.9-95.45 m. possibly an alteration halo to a pegmatite near hole. Indistinct contacts | | | | |
| 119.05 | 122.85 | PORPHYRITIC ANDESITE – as above | 2067551 | 119.05 | 119.1 | -volcanic → looks like typical GRV dacites<br>-zoned plagioclase phenocrysts<br>Amphibole phenocrysts (could have been pyroxenes now altered to amphibole but look like they could be original) |
| 122.85 | 123.8 | Medium grained k-spar-hornblende-biotite-plag with distinct amphibole needles. Possibly lamprophyric-basalt related. Traces pyrite and chalcopyrite | | | | |
| 123.8 | 134.1 | PORPHYRITIC ANDESITE – as for 112.88-118.47 m | 2067552 | 125 | 125.1 | |
| | | 134.1-146.2 m <u>INTERBANDED PORPHYRITIC ANDESITE AND PYROXENITE WITH MINOR DOLERITE BANDS</u> | | | | |
| 134.1 | 136.4 | PYROXENITE – grey-green, medium grained, plag-amphibole-biotite pyroxenite with traces of very fine grained pyrite and chalcopyrite, thin irregular anastomosing chlorite/ serpentenite veinlets and minor irregular carbonate veinlets | 2067553 | 135.7 | 135.8 | -intercumulate clinopyroxene (inclined extinction, orange XPL)<br>-olivine converted to serpentine<br>-more elongate grains also |

| Depth (m) (from) | Depth (m) (to) | Geology notes (adapted from Drill Hole Log DD88ME-2 by Palmer 1988) | Sample number | Sample depth (m) (from) | Sample depth (m) (to) | Thin section notes |
|---|---|---|---|---|---|---|
| | | 134.5-134.65 pegmatite band with chloritic or amphibolitic alteration halo and traces chalcopyrite and pyrite | | | | serpentinised may have been orthopyroxene |
| 136.4 | 140.87 | PORPHYRITIC ANDESITE – dark green to grey, fine grained dacite with plagioclase and rare k-spar phenocrysts and small biotite laths in very fine-grained quartzose groundmass. Rock fractured by very thin carbonate (?) veinlets. Lower contact is distinct with a chilled amphibolitic margin | | | | |
| 140.87 | 144.65 | PYROXENITE – grey-green to grey, medium-grained plag-amphibole-biotite pyroxenite containing rare traced fine-grained disseminated pyrite. Minor thin carbonate (?) veinlets and chlorite veinlets. Minor chloritic alteration, possibly related to dolerite dykes (?)<br>142.85-143.1 discordant hornblendite unit. Amphibole-chlorite-plag-biotite rock, possibly altered. Minor k-spar pegmatite remnant in centre, contacts gradational | | | | |
| 144.65 | 145.06 | ANDESITE – as for 136.4-140.8 m | | | | |
| 145.06 | 146.21 | ALKALI DOLERITE (?) – medium grained plag-k-spar-amphibole-pyroxene-biotite rock with amphibole forming distinct needles. K-spar usually forms in dominant sections. Altered pegmatite or alkali dolerite (?). Rare pyrite as fine disseminated euhedral grains. Distinct chilled upper contact | 2067554 | 145.4 | 145.5 | |
| 146.21 | 156.1 | CARBONATE ALTERED PORPHYRITIC ANDESITIC ALKALI BASALT – fine-grained, dark green-grey with small phenocrysts of k-spar and plag often altered to calcite (1-3 mm size and elongate, forming a weak foliation). Ground mass: very fine-grained mafic minerals and minor biotite. Lower contact chilled and irregular | | | | |

| Depth (m) (from) | Depth (m) (to) | Geology notes (adapted from Drill Hole Log DD88ME-2 by Palmer 1988) | Sample number | Sample depth (m) (from) | Sample depth (m) (to) | Thin section notes |
|---|---|---|---|---|---|---|
| | | 149.59-150.43 medium grained doleritic band with k-spar veinlets and xenoliths.<br>150.43-153.4 more andesitic interval with angular k-spar quartz gneiss and pyroxenite xenoliths. Rare thin carbonate veins | | | | |
| 156.16 | 158.1 | ANDESITE – fine-grained, light grey with k-spar and plag and rare biotite laths, in a quartzose groundmass. Rare thin chlorite veining. Indistinct lower contact. Core fractured | 2067555 | 156.35 | 156.4 | |
| 158.1 | 167.3 | CARBONATE ALTERED PYROXENITE – medium-grained, dark green-grey diorite consisting of equigranular mass of plagioclase, olivine (?) and laths of biotite with traces of very fine-grained disseminated euhedral chalcopyrite, variably altered by carbonate (calcite) replacing plag within rock and numerous thin veinlets which may contain chalcopyrite<br>158.1-159.35 pyroxenite contains extensive chlorite veining<br>159.35-159.5 thin pegmatitic band with chloritic or amphibolic alteration halo of surrounding pyroxenite<br>163.75-165 moderately carbonate altered section<br>165-167.3 strongly carbonate altered section | 2067556 | 166.15 | 166.25 | |
| 167.3 | 170.7 | CARBONATE ALTERED PORPHYRITIC ANDESITIC BASALT WITH GNEISS XENOLITH – dark grey, very fine-grained andesitic basalt with small phenocrysts (up to 1 mm) of carbonate (after plag) in a mafic ground mass. Minor traces disseminated pyrite and chalcopyrite. Thin carbonate veinlets throughout. Phenocrysts form a vague lineation. In parts the basalt contains xenoliths of k-spar-quartz gneiss<br>170.25-171.7 xenolith (?) of medium- to fine- grained, well | | | | |

| Depth (m) (from) | Depth (m) (to) | Geology notes (adapted from Drill Hole Log DD88ME-2 by Palmer 1988) | Sample number | Sample depth (m) (from) | Sample depth (m) (to) | Thin section notes |
|---|---|---|---|---|---|---|
| | | foliated, quartz-k-spar-biotite-amphibole gneiss (?) with coarse-grained k-spar-quartz segregations, wisps and bands parallel to foliation. Traces pyrite and at 170.8-170.9 carbonate altered dolerite with chilled margins. Irregular contact | | | | |
| 170.7 | 172.75 | BRECCIA/ SHEAR ZONE | | | | |
| 172.75 | 182.2 | CARBONATE ALTERED PYROXENITE – grey to grey-green, medium-grained pyroxenite, weak to strongly carbonate altered with carbonate replacing plag grains, shattered in parts by fine networks of calcite veinlets. Rare k-soar-quartz-amphibole pegmatite bands (up to 15 cm thick) with distinct chloritised pyroxenite margins (up to 15 cm wide). Rare traces pyrite and chalcopyrite as disseminated grains<br>172.75-173.7 strongly carbonate altered and veined interval<br>175.05-176 strongly carbonate altered section<br>176-176.15 pegmatite band with traces pyrite and chloritic altered pyroxenite margins<br>176.15-177.3 strongly chlorite and amphibolitic (?) altered section with minor biotite and chalcopyrite<br>179.15 thin carbonate veinlet with pyrite and pyrrhotite blebs<br>178-180.2 less altered pyroxenite<br>180.2-180.55 carbonate and chlorite altered pyroxenite with chlorite veinlets | | | | |
| 182.2 | 199.3 | CHLORITE ALTERED PYROXENITE – medium-grained, grey-green, biotite-plag-amphibole-chlorite pyroxenite with rare pyrite, chalcopyrite, and pyrrhotite as disseminated grains throughout. Minor talc coated joints. Pyroxenite variably | | | | |

| Depth (m) (from) | Depth (m) (to) | Geology notes (adapted from Drill Hole Log DD88ME-2 by Palmer 1988) | Sample number | Sample depth (m) (from) | Sample depth (m) (to) | Thin section notes |
|---|---|---|---|---|---|---|
| | | chloritically or amphibolitic altered throughout. Minor k-spar-quartz pegmatite bands with intensely chloritised haloes<br>182.2-185.1 strongly to totally chloritised section with carbonate veinlets and amphibole-rich sections. Minor talc, with fractured and brecciated quartz vein from 183-183.5<br>187.7-187.8 thin k-spar/ quartz band with chloritic alteration haloes<br>188.7-189.6 very strongly chloritic and talc altered sections<br>190-191.15 very strongly chloritic section<br>191.15-191.75 k-spar-quartz pegmatite band<br>191.75-193.3 strongly chloritic and carbonate altered pyroxenite with thin carbonate veinlets<br>193.3-193.7 pegmatite band<br>193.7-196.3 moderate to strong chloritic altered and moderate carbonate altered pyroxenite, rare traces chalcopyrite and moderate thin carbonate veinlets<br>196.3-199.3 weakly chloritically altered pyroxenite | | | | |
| | | 199.3-302.5 m <u>PYROXENITE WITH K-SPAR-QUARTZ PEGMATITE BANDS AND RARE DOLERITE</u><br>medium-grained, dark grey to grey-green, amphibole-biotite-plag pyroxenite. Weakly chloritically and carbonate altered in parts. Traces disseminated chalcopyrite and pyrite throughout. Minor to moderate, thin irregular carbonate veinlets. Minor talc on joint facings. Pyroxenite fractured and altered by k-spar-quartz pegmatite bands, pyroxenite next to pegmatite bands intensely chloritised. Very rare xenoliths of quartz-k-spar porphyry and k-spar-quartz-biotite gneiss. | 2067557 | 201.5 | 201.6 | |

| Depth (m) (from) | Depth (m) (to) | Geology notes (adapted from Drill Hole Log DD88ME-2 by Palmer 1988) | Sample number | Sample depth (m) (from) | Sample depth (m) (to) | Thin section notes |
|---|---|---|---|---|---|---|
| 203.5 | 205.3 | chloritic altered section with discontinuous pegmatite bands to 20 cm thick | | | | |
| 205.3 | 206.4 | chloritic altered section with thin carbonate veinlets | | | | |
| 206.4 | 206.7 | as at 203.5-205.3 | | | | |
| 206.7 | 209.6 | pyroxenite | | | | |
| 209.6 | 212.3 | intensely chloritised section with discontinuous wisps and bands to 50 cm of quartz-k-spar-biotite-chlorite porphyry. Porphyroblasts of k-spar to 4 mm. biotite forms a crude foliation with maybe contorted in parts | | | | |
| 212.3 | 220.2 | pyroxenite | 2067558 | 218.8 | 218.9 | |
| 220.2 | 220.7 | chloritised pyroxenite with pegmatite bands containing talc | | | | |
| 221.1 | | quartz-talc band | | | | |
| 222.3 | 223.8 | Chloritised pyroxenite with irregular pegmatite bands. Minor talc | 2067559 | 223.8 | 223.9 | |
| 223.8 | 227.8 | pyroxenite with chloritically altered sections surrounding pegmatite bands to 30 cm thick | | | | |
| 230.15 | 230.35 | pegmatite band with chlorite halo | | | | |
| 231 | 231.3 | as above | | | | |
| 231.75 | 231.9 | as above | | | | |
| 232.9 | 233.6 | As above | | | | |
| 243.4 | | Thin pegmatite band | | | | |
| 235.6 | | As above | | | | |
| 236.9 | 239.8 | Pyroxenite chloritically and carbonate altered in parts with pegmatite bands at 237-237.1 and 238.25-238.45. talc with pegmatite bands | | | | |
| 240.7 | 240.75 | pegmatite band with chlorite alteration haloes | | | | |

| Depth (m) (from) | Depth (m) (to) | Geology notes (adapted from Drill Hole Log DD88ME-2 by Palmer 1988) | Sample number | Sample depth (m) (from) | Sample depth (m) (to) | Thin section notes |
|---|---|---|---|---|---|---|
| 241.7 | 241.85 | As above | | | | |
| 242.1 | 242.3 | As above | | | | |
| 244.3 | 244.7 | As above | | | | |
| 245 | 245.15 | As above | | | | |
| 245.75 | 246.2 | As above | | | | |
| 246.2 | 247.8 | weak to moderate carbonate altered pyroxenite with thin carbonate veinlets containing traces chalcopyrite | 2067560 | 247.1 | 247.6 | |
| 247.8 | 248.1 | distinct fine-grained mafic band with chloritised garnets (?) | | | | |
| 248.1 | 249 | carbonate altered pyroxenite | | | | |
| 249 | 250.75 | Dolerite (?) medium- to fine-grained, green-grey, feldspar-biotite-pyroxene rock with clasts of k-spar-quartz-biotite gneiss. From 250 m amphibole phenocrysts | | | | |
| 250.75 | 252.5 | strongly chloritically and variably carbonate altered pyroxenite with clasts and wisps of k-spar-quartz gneiss | | | | |
| 252.5 | 257.7 | pyroxenite | | | | |
| 257.5 | 257.6 | fractured quartz chlorite vein or band | | | | |
| 259.75 | 260 | pegmatite band | | | | |
| 260 | 260.6 | Chlorite altered pyroxenite | | | | |
| 260.6 | 269.05 | pyroxenite | 2067561 | 267.1 | 267.2 | |
| 269.05 | 269.1 | quartz-plag-amphibole-chlorite pegmatite band | | | | |
| 269.1 | 270.6 | Pyroxenite | | | | |
| 270.6 | 270.7 | amphibole-plag-quartz-carbonate pegmatite band | | | | |
| 270.7 | 279.9 | pyroxenite | | | | |
| 279.9 | 282.3 | very weakly chloritically altered pyroxenite with chlorite-plag vein at 280.9-281.1 m | | | | |
| 282.3 | 285.4 | Pyroxenite | | | | |

| Depth (m) (from) | Depth (m) (to) | Geology notes (adapted from Drill Hole Log DD88ME-2 by Palmer 1988) | Sample number | Sample depth (m) (from) | Sample depth (m) (to) | Thin section notes |
|---|---|---|---|---|---|---|
| 285.4 | 287 | core fractured with weak carbonate alteration and veining | | | | |
| 287 | 292.55 | pyroxenite with fine wispy carbonate veins | | | | |
| 292.55 | 294.6 | pyroxenite with rare thin chloritic shear zones and weakly chloritic altered | | | | |
| 294.6 | 295.9 | Pyroxenite | | | | |
| 295.9 | 296.4 | k-spar-quartz pegmatite band | | | | |
| 296.4 | 300.3 | pyroxenite | 2067562 | 297.8 | 297.9 | -olivine altered to serpentine (clear mineral with dark black spots/lines, pale blue in XPL)<br>-cumulative texture<br>-orthopyroxene islands in clinopyroxene (brownish in XPL) |
| 300.3 | 303.1 | carbonate altered pyroxenite | | | | |
| 301.1 | 302.5 | pyroxenite | | | | |
| | 302.5 | END OF HOLE | | | | |

# APPENDIX C: FULL METHODS

## Choosing core and taking samples

SARIG was used to find drillholes that intersected GRV, with assistance from Claire Wade. These were then further assessed for rock types that were intersected, with particular interest in those holes that showed progression from mafic, through intermediate, to more felsic rocks. Those that showed some variation were looked at more closely using existing drillhole logs and reports available on SARIG. One was found to be suitable, with pyroxenite grading through andesite and dacite to a rhyodacitic material, with interlayers of basalt. While the available information suggested the core was moderately altered throughout, this was the most ideal hole to use based on the succession. This hole is located on the Labyrinth 1:50K (Kingoonya 1:100K) map sheet, on the north-western edge of Lake Labyrinth, near Kingoonya, SA.

The core was requested for inspection at the Glenside Core Library. During inspection, the core was roughly re-logged, using the existing log as a guide. This was done using a pencil and gridded paper on a clipboard, with the aid of a hand lens and a spray water bottle to make minerals easier to identify. Overall, not much was written on this log, as the existing log contained almost all the relevant information, though some rock-type identification required updating. Eighteen samples were chosen based on two main criteria: rock-type variation, and lack of veining. The desired samples were marked and labelled, before being cut by the staff at the core library. Removal of the samples from the core library was under the provision of the Mining Act 1971 and the Sample Removal Conditions set out by DMITRE.

Six polished thin sections were made from the samples taken from the core. The samples used were 2067547, 2067548, 2067549, 2067551, 2067553, and 2067562. A transmitted light microscope was used to look at the thin sections.

## Previously prepared samples

Due to the nature of this project, building on the work of Stewart (1994), some previously analysed and prepared samples were able to be reanalysed without extra

preparation time. Nine thin sections were analysed with the microprobe, to give more information about phenocryst compositions versus groundmass compositions. Previous geochemical analyses were also used to provide input for modelling programs.

In additions to this, two mineral separates were obtained from another honours student, Max Reddy. These were from GRV rocks that contained abundant zircons. The zircons were mounted and CL images were taken before lasering the zircons. This was done in two stages, to obtain age estimates and also trace element abundances.

**General sample preparation**

The samples taken from the core were used primarily for geochemical analysis from powders. The procedure was as follows:

JAW CRUSHER

To reduce the samples to chips and powder:

1. Clean – using compressed air, a wire brush, and ethanol and paper towel, checking for any caught fragments and dust

1.1. Blow off top with compressed air

1.2. Open top and middle door of housing, open jaws and blow off each section

1.3. Scrub jaws with wire brush

1.4. Blow off any loosened dust

1.5. Check for lodged fragments and remove with hacksaw blade if necessary

1.6. Squirt with ethanol and wipe with paper towel to geochemically sterilise the jaw/ teeth

1.7. Blow off again to dry out any remaining ethanol

1.8. Remove collection tray, blow out and wipe with ethanol and paper towel

2. Close jaws and lock in place with the side screw-wheel
3. Place paper at front of collection tray, slide back into place
4. Check spacing of jaws – adjust if necessary by using the wheel at the front of the jaws
5. Close doors of the crusher housing and lock

6. Turn on using the green START button
7. Drop sample into opening at top, quickly closing the chute to prevent fragments escaping
8. Listen for crushing of sample
9. Turn off using red STOP button when crushing sounds have stopped
10. Unlock doors and open
11. Remove catcher with sample in it
12. Use paper to lift crushed sample out
13. Place sample on paper aside, repeat cleaning steps

VIBRATING MILL (10G TUNGSTEN CARBIDE MILL HEAD)

To reduce crushed sample to a fine powder.

1. Locate correct mill vessel size – due to size of samples from core, the 10g mill head is used
2. Clean mill pieces – using compressed air, ethanol and paper towel – starting with the main bowl so that the puck can be placed inside once it is clean, rather than on the bench where it may be contaminated

2.1. Blow off with compressed air
2.2. Squirt with ethanol and wipe with paper towel to geochemically sterilise the mill pieces
2.3. Blow off again to ensure pieces are dry
2.4. Run mill with quartz before sample to ensure any contamination will be known
2.5. Clean again after each sample

3. Pour crushed sample into the mill between the puck and the edge of the bowl, wiping off any that falls on top of the puck – some samples were milled in two stages, as they were a little too big to be milled in this size vessel all at once, but still not big enough to go up to the next vessel size
4. Place lid on, ensuring that it is on properly so no sample will escape
5. Check correct sized base is on the vibrating mill, so that the vessel can be securely clamped down
6. Place vessel on base – layer piece of rubber and carpet on top to ensure clamp will be firm

7. Clamp down the mill with the handle, ensuring the rod goes between the notches and folds down securely (keep in place by sliding up the zip tie)
8. Close the lid of the housing
9. Set timer (e.g. for one minute)
10. Press start
11. When finished, wait for machinery to stop moving, then open housing
12. Unclamp and remove the mill vessel and carefully open, with the aid of a hammer if necessary, without spilling any of the powder
13. Tip powder and puck onto clean paper
14. Remove puck and place in main bowl
15. Check powder for fineness and consistency of fineness

15.1. If not milled completely (still feels gritty when rubbed between two fingers), pour back into mill and run again

15.2. If milled sufficiently, pour sample into clean and labelled sample bag

16. Repeat cleaning steps

16.1. If sample cakes, can run mill with quartz to aid cleaning

ZIRCON MOUNTS

Some zircons from the mineral separates taken from Max Reddy were mounted using the following procedure:

1. Clean glass slide with ethanol and tissue
2. Stick piece of double-sided tape on glass slide (as much as possible, prevent or remove bubbles). Keep backing
3. Place piece of single-sided tape over double-sided tape (sticky side up) and use backing from double-sided tape to smooth out bubbles
4. Use silicon mount (inside rim) to trace a circle into the glue on the tape with the pick (this is where zircons will be mounted), choose an area that is most smooth
5. Clean a petri dish with ethanol and tissue

5.1. Cover base of dish with ethanol, tip in bin and wipe dry with tissue

6. Tip mineral grains into the petri dish
7. Set up two binocular microscopes close together
8. Place the petri dish of grains under one and glass slide with tape under the other
9. Position the glass slide so that the circle that was traced in the glue can be seen

10. Use a pick (touch on face to make oily so grains will stick) to pick up zircons and transport them to the sticky circle

10.1. Make 3 lines of zircons relatively close together, but not touching

11. Use double-sided tape backing to cover the zircons until ready to glue

12. Print off short labels (size 9 font) and cut out

13. Prepare glue

13.1. Mix 5g of epoxy resin with 1g of hardener for each mount (2 mounts = 10g of epoxy resin, 2g of hardener – can be prepared together)

13.1.1. Place plastic cup on scale (cover scale with paper towel to assist clean up if spill occurs)

13.1.2. Tare scale

13.1.3. Pour 10g of resin into cup

13.1.4. Tare scale

13.1.5. Pour 2g of hardener into cup (use a second cup to assist slow pouring)

13.1.6. Mix well with pop stick

13.1.6.1. Will become cloudy, then clear again (clear = ready)

13.1.6.2. If bubbles appear, heat for 2 minutes in low temperature oven (bubbles will rise to the surface and pop)

13.2. When glue is sufficiently mixed, remove backing tape from glass slides and place silicon moulds over the area where zircons are mounted

13.3. Slowly pour glue into moulds until at approx. 1cm thickness

13.4. Carefully place sample labels onto the surface of the glue with tweezers (sample name/number up)

13.5. Leave to set overnight

14. Polish mounts

14.1. Polish side with zircons

14.2. Use 1000 grit paper by hand for approx. 2 minutes in figure 8 patterns to ensure even polishing

14.2.1. Check surface under binocular microscope and continue polishing until surface of zircons is at surface of mount

14.3. Use 2400 grit paper by hand in figure 8 patterns until surface is evenly smooth and as many zircons as possible are exposed at the surface

14.4. Use the cloth lap to polish mount surfaces more (follow available instructions about which cloth to use with which diamond paste)

14.4.1. Use the blue cloth (3um) with green diamond paste for about 10 minutes on low speed

14.4.2. Use the brown cloth (1um) with blue paste for about 10 minutes on low speed

14.5. Clean mounts with ethanol and tissue, also advisable to use a sonic bath for 5+ minutes to remove as much diamond paste as possible

14.6. Wrap clean and polished mounts in Kimwipes for transport

**Analyses**

As the goal was to run the *Rhyolite-MELTS* program, the information required for the program was obtained. This includes major and trace element analyses. Interest was also in REE values.

PHILIPS XL40 SCANNING ELECTRON MICROSCOPE - CL IMAGING OF ZIRCONS

1. Getting started

1.1. Dual monitor set up – monitor on right known as *XL Control* (for movement of stage, turning on the electron beam, etc.); monitor on left used for acquisition of EDS spectral data

1.2. On the *XL Control* monitor, double-click the 'Microscope control' icon. Microscope control screen will appear

2. Inserting sample

2.1. Ensure sample holder is at maximum working distance by selecting 40 mm from the drop down menu and the "GoTo" button

2.2. Then go to the vacuum control group and click 'Vent' button

2.3. Wait approx. 2 minutes before attempting to open the door using the bar on the bottom of the front of the chamber. If the door does not budge, the chamber is still venting.

2.4. Insert a sample or samples into appropriate holder and use carbon tape to secure

2.5. If the backscatter detector is required, check that it is inserted correctly

2.6. Close door and hold closed while selecting 'Pump' button from the vacuum control group

2.6.1. If a whooshing sound is heard, the door is no closed properly. Lift and push the door slightly

3. Obtaining an image

3.1. Before turning the microscope one, in the 'Microscope Control' window, use the pull-down menus to select operating parameters suitable for the sample to be examined

3.1.1. Beam: from this menu, you can select the required acceleration voltage and spot size required for your samples. Typically, low kV for non-conducting samples (5-10 kV) and medium to high kV (15-20 kV) for conducting samples. Spot size indicates how much current is applied to the sample, and for initial magnification viewing should be set around 4 or 5

3.1.2. Magnification: this menu selects the magnification of your sample. Initially it is best to use the lowest magnification possible. Magnification can also be adjusted with the + and – keys on the number pad of the keyboard. If different default magnifications are required they can be adjusted with the 'Magnification presets…' option in this menu

3.1.3. Scan: this drop down selects the speed at which the electron beam rasters across the field of view (equivalent to the refresh rate of a monitor). For initial viewing purposes, select 'TV' mode which is approximate to real time viewing of the sample. Note: if using the backscatter detector, NEVER use TV mode as damage to the sensitive detector may occur. Always use slow scan 1, 2 or 3 with BSE mode (see section 3.1.3). For imaging purposes, slower scan rates are selected to improve picture quality (see section 4 – optimising the image). In addition to this, the user has the option of selecting the Scan mode. For general viewing purposes, this should be set to full frame, however specific tasks, such as general image optimisation, will require different modes (see section 4 – optimising the image)

3.1.4. Detectors: this menu allows the user to select which detector is to be used. For initial start-up, before the electron beam is turned on, the secondary electron detector (SE) should be selected.

3.1.4.1. Secondary electron detector (SE): secondary electrons are very low energy electrons (<50 eV) emitted from the outer shell of atoms comprising the material of

interest due to excitation by the primary electron beam. Due to their low energy, only secondary electrons from the first few atomic layers of the material (few nm) can escape and as such SE mode reveals information on surface topography of the sample. Secondary electrons from topographic highs are more easily emitted and do not have to travel as far to the SE detector, thus appear as bright spots, and conversely topographic lows appear as dark regions due to the lower number of electrons emitted

3.1.4.2. Backscattered electron detector (BSE): incident electrons from the electron beam can also be elastically scattered by close encounters with the dense atomic nuclei. As such back scattered electrons are high energy electrons scattered from atoms up to about 50 nm below the surface of the sample (measured in keV – they have approx. the same energy as the incident electron beam). As a result, BSE mode reveals information on the Z contrast of your sample (Z=atomic number) where regions that contain material with a high Z will be viewed as bright regions and conversely atoms with a low Z as dark regions. Note: make sure TV mode is NOT selected under the scan menu

3.1.4.3. CCD camera: this option will display an image of the inside of the sample chamber via the CCD cameras mounted on the XL40. This option is useful when rotating the stage or adjusting the sample height to make sure you are not driving your sample into the pole piece or backscatter detector if mounted. The CCD camera is vital when employing the cathodoluminescence (CL) detector (see section 7 – CL imaging)

3.1.4.4. IMG: again, this option is used for CL imaging and is explained in section 7 – CL imaging

3.1.5. Filter: from this menu, the user can select the frame store noise-filtering mode. As a general rule, is using slow scan speeds, the live noise filtering mode should be selected and if using TV mode, then average 4 and standard definition can be selected.

3.1.6. Once all these settings have been selected, we are now ready to turn the electron beam on

3.2. Control Area

3.2.1. Settings: once the vacuum is sufficient to turn the electron beam on, the ‘Vac OK’ status is indicated in Vacuum Control Group. Make sure that the SE detector is

selected then click on the kV button (in Beam control group) to turn the beam on. Once turned on, this button will be highlighted yellow and an image should appear on the screen. If screen remains black, the contrast and brightness settings may need to be adjusted. As a starting point, adjust the contrast and brightness using the automatic contrast and brightness (ACB) button (in button bar or button in Settings control group). The sliding controls in the Settings control group can also be used. Note: ACB cannot be used if the backscatter detector is selected. When the beam is turned on, a dialogue box 'Microscope confirm focus' will appear in the screen. After finding the highest part of the sample, increase magnification to 500 or more. Carefully focus the image (see section 4.3) and press OK in the dialogue box. This links the working distance (WD) in the data bar to Z height in the stage control group. Note: it is very important to carry out this procedure before proceeding in order to avoid possible damage to the microscope or sample when changing working distance. Once the working distance is calibrated, drive the stage to the optimal height of 10 mm from the Z drop down box and 'GoTo' button (for CL (see section 7) this height must be no closer than 15 mm for best results, use a WD of 15-16 mm).

4. Optimising the image

4.1. Adjusting contrast and brightness: as a starting point, it is good to use the ACB function. However, the contrast and brightness can be adjusted manually via the slider bars on the 'Settings' and 'Stage' tabs of 'Microscope Control', and it is recommended that these are utilised to obtain the optimum image for the material of interest. If the sample of interest displays large contrasts of shades of grey, one method to optimise your image is by using the Horizontal Line function. Navigate to a feature of your sample that contains the largest contrast variation and select the Horizontal Line function and Slow Scan 3 from the Scan drop down menu. The screen will now display a solid white horizontal line bounded by two dashed white lines, along with a spiky white line. The incident electron beam is now scanning along the solid white line, and the spiky white line is an output of the "brightness" of the pixels along that solid white line, where the uppermost dashed white line represents pure white, and the lower pure black. Generally, you want the spike bright line to sit just within the bounds of the upper and lower dashed lines to maximise the contrast of your image to pull features out, while minimising areas of

pure white and black. As such, the 'Contrast' slider bar will stretch the spiky white line, and the 'Brightness' slider bar will shift it up and down. Once this is done, click "Save ACB Settings"

4.2. Moving the sample: to move around your sample, select the 'Track' button in the button bar (looks like a target with a line coming out to one side). Place the cursor between two concentric circles, and hold down the LH mouse button. The sample will move in the direction of the vector. The speed of movement is proportional to the distance of the cursor from the inner circle. Move to a section of sample that displays some detail that can be focused on.

4.3. Rotating the sample: to rotate the sample, open the 'Stage' control group in the 'Imaging' control area (arrow in top RH corner). By moving the sliding control, the sample can be rotated in either direction. The speed of the rotation is indicated by the arrows above the control. The image of the sample can also be rotated by using the 'Scan rotation' sliding control. In addition to this, the coordinates of locations of interest can be stored if you need to return to them. Simply type in the label you would like to give the position and click 'Add'. A cross in the stage schematic will mark the positions located. To return to a position simply double click on the name of the positon in the list.

4.4. Focusing: once the beam is turned on, the image needs to be focused. To do this, zoom out to the lowest magnification and hold down the RH mouse button (horizontal double arrow appears). Whilst holding down the RH mouse button, move the mouse slowing left or right until optimum focus is achieved. Once this is done, repeat the steps of zooming in and focusing until image is focused at required zoom of work. Note: Slow Scan 1 should be used whilst focusing to obtain optimum image.

4.5. Astigmatism correction: Ideally, when the electron beam hits the surface of your sample it should have a circular cross-section. However, due to the effects in the lenses and/or contamination in the column, the beam can vary in shape and commonly forms an ellipse. This is called astigmatism, and the higher magnifications can produce artefacts in the image obtained. As such, astigmatism must be corrected before the best possible image can be obtained. To correct for this, we apply a magnetic field to the electron beam to adjust its shape. Focus at high magnification as described above. Click and hold the LH mouse button in the

'Stigmator' box ('Imaging' control group), which will display cross hairs over the image. Move one cross hair over the image until the clarity improves. Then, while holding position of the cross hair, repeat the process with the other cross hair. Refocus the image. Astigmatism can also be adjusted by holding down the Shift key while holding down the RH mouse button.

4.6. To tilt the sample: if tilting of sample is required, open the 'Stage' control group in the 'Imaging' control group and adjust the value of T (tilt). As you are tilting, make sure not to crash your sample into the pole piece of the backscatter detector if installed. As a guide, do not tilt over 26 degrees. Make sure the CL detector is retracted before tilting.

5. Image storage

5.1. Data bar: in the 'In/Out' menu, select 'Databar Setup'. The information in the data bar can be altered by selecting or deleting various items. A text box is displayed, in which information about the sample can be entered. If the 'Background' box is selected, the data bar will appear as white writing on a black background. If not, the background will be clear. When complete, click on 'OK'.

5.2. Storing the image:

5.2.1. In the 'In/Out' menu, select 'Image'

5.2.2. Select the TIFF file option, and in the textbox type in a filename up to eight characters long in place of the * symbol. Note: no spaces are allowed in the file name.

5.2.3. Click on the 'Save' button. A time-lapse bar will appear, and the image will be saved to the server. The screen will be restored to normal when the function is complete. Note: if the information in the data bar is required for images that are to be accessed remotely, click on the 'Databar on image' box before saving. The data bar will then become a permanent part of the image

5.3. Restoring an image: to review images already stored, select 'Image' in the 'In/Out' menu. Select the required image from the file by clicking on it, and it will appear in the text box. Click on the 'Restore' button, and the stored image will be displayed.

6. CL imaging

6.1. Sample insertion

6.1.1. Make sure the stage has been lowered to 40 mm and vent the XL40 chamber as described in Section 2. If not already done, make sure the stage is at 0 degrees tilt

and the CL detector is wound all the way out (turn blue knob on the Gatan CL detector fully clockwise)

6.1.2. Open the door and insert the sample. Close the door and 'Pump' the vacuum chamber as described in Section 2. When 'Vac OK' has been achieved, turn on the kV (use 12kV, spot size 7). Select SE from the 'Detector' drop down menu and turn the beam on (as described in Section 3.2.1)

6.2. Focusing

6.2.1. Move around to the desired area of interest and focus on your sample as clearly as possible, then link the working distance

6.2.2. Select 'CCD' from the 'Detector' pull down menu and bring the stage up to 15-16 mm (no closer than 15 mm) by changing Z and clicking 'GoTo'. Watch the CCD camera view as the stage is raised

6.2.3. Again, focus on your sample as clearly as possible, then link the working distance (WD). Then change Z to 16-16 mm again and click 'GoTo'

6.2.4. While watching the CCD camera view, wind in the CL detector (turn the blue knob on the Gatan CL detector counter clockwise), making sure that there is enough clearance between the CL detector and the top of your sample. The gap between the detector and sample should be very small (around mM) but there needs to be one. If it looks like it will collide with anything, you will need to wind the CL detector back out, refocus, relink the WD, change the stage height to a higher value (over 15 mm), and try again. The height of the sample will need to be adjusted such that the sample surface is 7.66 um (Y direction) using the measurement tool with the Microscope Control software

6.3. Imaging

6.3.1. Select 'Slow Scan 3' from the 'Scan' drop down menu, and 'IMG' from the 'Detector' drop down menu

6.3.2. On the CL power panel, turn the power on by hitting the 'Power' switch at the top LH corner of the panel, and increase the HT to between -500 and -650 until an image appears (around -600 is usually OK, but do not exceed -650)

6.3.3. Adjust the brightness and contrast of the image using the Horizontal Line scan function as explained in Section 4.1, however use the brightness and contrast knobs on the CL control unit instead of those within Microscope Control

6.4. Closing down CL

6.4.1. Decrease the HT on the CL detector control back to zero

6.4.2. Power OFF the CL detector

6.4.3. Ensure that the CL detector is wound all the way out by turning the blue knob on the Gatan CL detector fully clockwise

6.4.4. Vent chamber and remove sample as per shutdown procedure detailed in Section 7

7. Closing down

7.1. Make sure the SE detector is selected and turn beam off by clicking on kV button in 'Beam' control group

7.2. Drive the stage down to its maximum working distance of 40 mm. vent chamber by clicking on the 'Vent' button. Once vented, door will not open automatically and as such after approx. two minutes gently attempt to open the door using the bar on the bottom of the front of the chamber. If the door does not budge, the chamber is still venting.

7.3. Remove samples from the chamber

7.4. Close the door and 'Pump' the chamber – wait until 'Vac OK' status is indicated

7.5. Close Microscope Control software

7.6. Collect data by copying to a USB drive

LA-ICP-MS

This methodology was performed on the zircon mounts.

1. Inserting samples

1.1. Ensure ICP-MS is in standby mode

1.2. Loosen the screws on the laser ablation chamber door and slide the door to the left. The sample holder will then slide out

1.3. Clean samples with ethanol and Kimwipes (remove as much carbon coating as possible)

1.4. Place samples into the cells of the sample holder, ensuring the samples are held securely and tops of the samples are level with the top of the holder (otherwise camera will not focus properly – can use Blu-tack and coins to bring up, or grind the base down if too high)

1.5. Insert the sample holder into the chamber, close the door and tighten the screws

2. Getting started and turning on gases

The operation of ICP-MS for laser ablation studies requires the user to setup two separate systems to use concurrently. There are three computers at the use console: left computer controls the Glitter Data Processing software (known as the *Glitter* Computer); the middle computer controls the ICP-MS through the ICP-MS Top software (known as the *Chemstation* Computer); and the right computer is used to view the samples and operate the laser ablation system (known as the *NewWave* Computer).

2.1. Start ICP-MS Top program [*Chemstation* Computer]

2.2. Select "Instrument Control" from the Instrument menu. Check the displays in the bottom of the screen and ensure the Argon Gas pressure reads above 500 torr (advise staff if it does not)

2.3. Select "Maintenance menu" then "Sample Introduction"

2.4. Check box "Optional Gas" and type 60% for "Optional Gas" and click on Enter

2.5. Open "Laser Ablation" program on the *NewWave* computer

2.6. Ensure "Online" is selected

2.7. Click on "Evacuate." A dialogue box will pop up with a status bar, indicating the number of cycles. The laser ablation chamber is being evacuated and then refilled with He in cycles

2.8. Once finished, click "Evacuate" two more times. The system needs to do a total of 30 cycles to remove all the air from the chamber (each time does 10 cycles)

2.9. Close "Sample Introduction" dialogue on the ICP-MS Top program. This will reset the optional gas to 0%

3. Turning on the plasma

3.1. In ICP-MS Top program, select Instrument > Tune

3.2. Select "Optional Gas" slider bar (probably set at around 58%) and turn it down to 20%

3.3. Select Instrument > Instrument Control

3.4. Select Instrument > Instrument Control > Start Plasma

When the plasma is ignited, the *Chemstation* will change mode of the system from Start Up mode to Standby mode. This can take a few minutes. If for some reason the plasma is extinguished the mode of the system will default back to the former mode, which will also take a few minutes.

3.5. Wait until the plasma is fully operational (all gauges green – approximately 2 minutes)

3.6. Go back to Instrument > Tune and turn Optional Gas back up to correct value (usually 58-59%)

3.7. May need to wait up to half an hour for the plasma to stabilise. This is a good time to set up the method and save the locations of samples

4. Load method

The method is the experimental parameters used by the mass spectrometer on the ICP-MS. It includes the elements to be analysed, the acquisition mode and acquisition times

4.1. On the *Chemstation* computer select the Methods menu > Load

4.2. Select BenZirc.M for zircon dating, JTZirc.M for trace elements in zircons and click ok

4.3. Choose the equivalent calibration file (with a C extension) and click ok (In Laser Ablation mode the calibration file is not used however the software will still require this file, if no equivalent calibration file can be found then select Default.C)

5. Setting up the laser ablation system

5.1. Open “Laser Ablation” program on the *NewWave* computer

5.2. Turn up light intensity and choose COAX mode of sample illumination

5.3. Choose 5 Hz for laser fire frequency/ rate

5.4. Select laser spot size 30 um

5.5. Select power rating 80%

5.6. In order to view the sample surface, the user can adjust the optical zoom. To locate samples use a zero value for the optical zoom, when using the laser increase the zoom to 50%

6. Saving the positions of standards

Standards used were the NIST Standard Block (NIST 610 and 612), Zircon Standard Block 1 (GJ and Plesovice), and Zircon Standard Block 3 when Block 1 was unavailable (GJ and BJWP)

6.1. Locate a standard, click “Position” button > name position > “set to current stage position” > “Add”

6.2. Do the same for the first points of your sample blocks

6.3. If the position of a standard or sample changes, select the relevant positon from the list and click “Edit” > “Set to current stage positon”

7. Tuning the plasma: P/A Factor

Tuning of the plasma, lens, and detector system is extremely critical for the equality of results. Once the plasma has been lit, the system is monitored using the Instrument Tune panel. Counts of Ar-Ar at mass 80 are used to determine the stability of the plasma. Hit the START button on the Instrument Tune panel to obtain mass signals. Stable counts of mass 80 higher than 2 million indicate that the plasma is stable.

The P/A Factor allows the ICP-MS software to process signals acquired by the detector in pulse count mode and analogue mode with seamless/ linear calibration/ this transition in the way the signal is measured occurs when counts per second exceed approximately one million. Thus the P/A Factor is not required every time the system is run, only when you expect cps to exceed approximately one million in your unknown (note: always perform P/A Factor if attempting geochronology, as counts per second in zircon and monazite typically exceed one million). When conducting a P/A Factor, what we are attempting to do is trip the detector into analogue counting mode by obtaining over one million counts in at least two elements at opposite ends of the mass spectrum you are analysing. We do this by increasing the spot size and intensity of the laser, and ablate a high concentration NIST glass.

7.1. Move to NIST 610 (dark blue glass)

7.2. Initially, change the beam to 65 um and increase frequency to 10 Hz (85% laser output)

7.3. To view counts on the detector of specific isotopes click the “Acq. Params” menu (acquisition parameters) and tick 80, 206, 248/232, 207, 208, 204, 238, 220, and click ok. These isotopes will now appear on the tune screen

7.4. Start laser firing, open shutter, click start on tune screen

7.5. When over one million counts in $^{238}U$ and $^{208}Pb$ click stop on the Tune panel. Select Tune > P/A Factor > click “Load Masses from acq. Method” > Run

7.6. When the notepad automatically pops up, check that $^{238}U$ and $^{208}Pb$ are in detection range (they will have a number next to them, usually about 0.9) then click “Yes” to new P/A Factor, click “Save”

7.7. Stop laser firing, close shutter

7.8. Turn settings back to normal (5 Hz for laser fire rate, 30 um for spot size and 85% laser intensity)

8. Running the method

The analytical method for Laser Ablation starts with the user running a number of standards. The first of these standards will be recognised by the Glitter software and when loaded into a Glitter processing session will be assigned a star (*) and data associated with them. The standards allow the calibration of laser ablation data in two ways: measure ablation yield and drift in signal over the period of the analyses and degree of fractionation. Some standards are run as unknowns. By analysing material of known composition or age, we can evaluate whether or not our selected standards analyses are valid.

Using the *Chemstation* computer:

8.1. Create a folder on the D: drive to store your data and relevant sub-folders for individual samples/ runs

8.2. Move the laser ablation cell to the first standard

8.3. Select “Method” > “Run.” Enter the path where the files are going to be stored (can be copied and pasted from Microsoft Explorer e.g. D:\username\samplename\) and add the name of the spot analysis to the end of this path (Chemstation creates folder of data with this name). For example the first spot analysis for zircon would be a GJ standard, and so the path filename would look like D:\username\samplename\GJ_01

8.4. Thus, for every spot after that for this specific sample you would only need to modify the spot name and leave the path directory as it is

8.5. Click “Run Method” and view the time elapsed value displayed on the screen. The first part of the run will be background. The laser is then fired and the shutter opened (background collection for 40 seconds, fire laser for 10 seconds and open shutter at 50 seconds total. At end of full 120 seconds, stop laser and close shutter.

8.6. Method must be run to full completion for the data to be saved. When completed it will exit back to the Tune screen

8.7. Data is now ready to be viewed in Glitter program

9. Using Glitter

9.1. Open the Glitter program from the desktop of the *Glitter* computer

9.2. Choose “isotope ratios” when conducting geochronology or “element concentration” when attempting trace element analysis

9.3. To load data files into Glitter, select “File” > “Load data” and navigate to the I: drive. This takes the data from the central computer across the network. Then navigate to the root directory where all your spot analyses are stored. Click ok

9.4. A window will pop up in which the user must set the detector dwell times, which have been setup in the method on Chemstation. For zircon geochronology, the following dwell times are used:

| Isotope | Dwell time in msec |
|---|---|
| 204 | 10 |
| 206 | 15 |
| 207 | 30 |
| 208 | 10 |
| 232 | 10 |
| 238 | 15 |

For trace element analysis in zircon, the following dwell times are used: Si, Zr, Th, U 10 msec; all other elements 20 msec

9.5. Click “Accept” twice, then ok to the box that pops up

9.6. Then choose “Display” > “Age Estimates” to display spot ages; or “concentration” for trace elements in ppm

9.7. Select “Review Signal Selection” from the “window” pull down menu. This window is where signal selection points can be altered to choose where signal and background counts are considered to be

9.8. Check that the ages/concentrations of the standards match those from the standard block selection

9.9. Now for every spot conducted the user simply needs to hit the “Update” button in Glitter, which will automatically bring the next spot analysis across from the central computer.

9.10. After a series of standards have been analysed, the Glitter program will prompt the user for a different routine for processing the standard/calibration data. To begin, choose “Linear fit to ratios” in the Windows Options drop down menu. Also select “Tie standard markers to analysis” in the second drop down list

10. Completing a run

10.1. Spot analysis was done under the following pattern to prevent the Glitter program from becoming overloaded and slowing down:

For geochronology (one run):

10.1.1. Std GJ x3

10.1.2. Ples or BJWP x2

10.1.3. Std GJ x2

10.1.4. Samples x20

10.1.5. Std GJ x3

10.1.6. Ples or BJWP x2

10.1.7. Std GJ x2

For trace elements (one run):

10.1.8. Std NIST 612 x3

10.1.9. GJ x1

10.1.10. Std NIST 612 x2

10.1.11. Samples x20

10.1.12. Std NIST 612 x2

10.1.13. GJ x1

10.1.14. Std NIST 612 x2

10.2. Data was then exported, Glitter program restarted, and the last set of standards copied into a new folder for use with the next run

11. Exporting data from Glitter

11.1. Once the required amount of data has been obtained (i.e. one run), select "File" > "Export" in the Glitter program

11.2. Leave the default boxes selected, additionally select "Mean Count Rates (cps), background subtracted" then click ok

11.3. Save the data to the default location (this will automatically be the same folder the program has loaded the original data from) and click "Save"

12. Shutting down the laser

12.1. In the ICP-MS Top program, select "Instrument" > "Instrument Control"

12.2. Turn off the plasma under the "Plasma" drop down menu or by hitting the "Plasma Off" icon

12.3. Shut down the Laser Ablation software on the *NewWave* computer. This turns off the light source in the laser unit and preserves the bulb

12.4. Turn off the monitors on all three computers. Do not shut down the computers

13. Removing samples

13.1. Loosen the screws on the laser ablation chamber door and slide the door to the left

13.2. Slide the sample holder out

13.3. Carefully remove samples and standards

13.4. Return sample holder to the chamber

SOLUTION ICP-MS

Method specific sample preparation:

1. Clean 15 mL PFA vials

1.1. Wipe outside of vials with ethanol and tissue to clean off previous sample labels

1.2. Pour a small amount (approx. 5 mm depth) recycled 6M HCl into each vial

1.3. Put lids on vials

1.4. Place vials on a hot plate set at 140$^{o}$C (in fume cupboard)

1.5. Leave for 30+ minutes

1.6. Switch off hot plate and remove the vials, placing them on a temperature suitable material to cool

1.7. Fill a 4L beaker with 2-2.5L of deionised water

1.8. Bring the vials and beaker to the same fume cupboard

1.9. Pour remaining HCl from the vials into a 'waste' jug

1.10. Place now emptied vials and their lids into the beaker of water

1.11. Dispose of waste HCl appropriately (in this case, into a larger container for waste HCl)

1.12. Drain water from beaker

1.13. Add vials to cleaning container for longer term cleaning

1.13.1. Take rack out of cleaning container

1.13.2. Place lids upside down on the top row of rods, place vials upside-down on the bottom row of rods

1.13.3. Return rack to container, secure the top half (lid)

1.13.4. Remove the stopper from the funnel at the top

1.13.5. Ensure drainage spout is closed

1.13.6. Pour 1L of 69% nitric acid into a measuring jug and then into the container via the funnel. Rinse measuring jug with deionised water

1.13.7. Reinstate stopper, but leave the stopper loose to prevent pressure build up within the container

1.13.8. Switch on hotplate beneath the container – set to 170$^{o}$C

1.13.9. Leave overnight, then switch off hot plate and allow the container to cool for approx. 30 minutes

1.13.10. Drain nitric acid into measuring jug by opening the spout and return to original Winchester (can be reused up to 20 times for this purpose). Update the number of uses marked on the Winchester. Rinse measuring jug with deionised water and ensure spout is reclosed

1.13.11. Pour 1L deionised water from a measuring jug into the container via funnel

1.13.12. Leave with hotplate at 170$^{o}$C for approx. 8 hours (i.e. during day), then switch off hot plate and allow to cool for approx. 30 minutes

1.13.13. Drain water into measuring jug by opening spout and dispose of appropriately (pour down drain) and close spout

1.13.14. Measure out 1L 37% HCl into a measuring jug and pour into container via funnel and return stopper

1.13.15. Leave with hot plate at 170$^{o}$ for approx. 2 days

1.13.16. Drain HCl into measuring jug and return to original Winchester. Update the number of uses marked on the Winchester. Close spout and refill container with 1L deionised water. Leave for approx. 2 days

1.13.17. Drain water and dispose. Remove rack with vials and lids and place on open bench space

1.14. Flick excess water off vials and caps and lay out on clean bench

1.15. Fill each vial with approx. 0.5 cm depth 6M HCl and put lids on

1.16. Place vials on hot plate at 140$^{o}$C and leave for approx. 24 hours

1.17. Remove vials from hotplate and allow to partially cool. Tip out HCl into a beaker (ok to reuse) and rinse vials/ lids with deionised water. Check for areas where water clings to the sides of the vials – mark these vials with an 'x' and only use if you have to

1.18. Cap rinsed vials and place in clean, labelled tub ready for weighing

2. Weighing

2.1. Use Mettler Toledo AT201 balance in air lock room B13

2.1.1. Long and short term stability of the scale is monitored for all weighing sessions by first weighing a standard 100g weight from the weights box and recording this in the log book

2.2. Label a 15 mL vial with black marker pen and record label in log book

2.3. Uncap the vial and hold with the balance tweezers. Use the Zerostat gun to remove static charges by holding it approx. 10 cm from the vial and slowly squeezing and releasing the trigger over about 4 seconds. If a 'crack' sound is heard, repeat more slowly.

2.4. Place vial on balance and tare

2.5. Use a spatula to add approx. 0.05g of powdered sample to the vial. Record in log book to 4 decimal places

2.6. Remove vial from balance, add approx. 2 mL 7M $HNO_3$ and cap vial

2.7. Record all weights, etc. in the log book

2.8. Repeat for all samples

2.8.1. Include at least one rock standard and one blank (blank does not have sample to be weighed, but needs to have the 2 mL 7M $HNO_3$ added)

2.9. Repeat weighing of the standard 100g weight and record in log book

3. Dissolution of sample powders

3.1. Add 4 mL of HF from the dispenser into each vial

3.2. Heat capped vials overnight on a hotplate set to 140$^{o}$C

3.3. Remove vials from hotplate and allow to cool slightly to make them more comfortable to handle

3.4. Gently tap the vials at a slight angle to collect any acid drops from the top or sides

3.5. Remove caps and return vials (and caps upside-down) to the hotplate to evaporate to dryness at 140$^{o}$C for approx. 2 hours (add approx. 2 mL of 7M $HNO_3$ when nearly dry to prevent insoluble fluorides forming).

3.6. Allow to cool, then add 4 mL HF + 2 mL 7M $HNO_3$

3.7. Recap and heat overnight at 140$^{o}$C on a hot plate

3.8. Again, remove vials from hotplate and allow to cool slightly to make them more comfortable to handle

3.9. Gently tap the vials at a slight angle to collect any acid drops from the top or sides

3.10. Remove caps and return vials (and caps upside-down) to the hotplate to evaporate to dryness at 140$^{o}$C for approx. 2 hours (add approx. 2 mL of 7M $HNO_3$ when nearly dry to prevent insoluble fluorides forming).

3.11. Allow to cool, then add 6 mL HCl to the solid residue

3.12. Heat capped vials on hotplate at 140$^{o}$C until completely dissolved (overnight)

3.13. Allow to cool to room temperature and assess solutions for remaining solids (may need to repeat evaporation processes)

4. Centrifuge

4.1. Evaporate to dryness on a 140$^{o}$C hotplate

4.2. Cool, then use the balance to add 5mL of 5% $HNO_3$ + 0.1% HF mix to each vial while on the balance, record the weight of acid added and leave to dissolve. This produces a 100x dilution factor (dilution factor 1)

4.3. Rinse 2 mL centrifuge vials (stored in 6M HCl) three times inside and out with DI water and store in rack

4.4. Place rack on hotplate set to 120$^{o}$C to speed up drying

4.5. Pipette 1.5 mL of each solution into labelled centrifuge vials

4.6. Using the Micro Centrifuge in room B14, centrifuge the samples for 5 minutes at 13200 rpm

5. Dilution

5.1. Using the balance to obtain more accurate weight measurements at each stage; pipette 0.5 mL of the centrifuged sample solution into a 5mL ICP-MS vial

5.2. Add 4.5 mL 5% $HNO_3$ + 0.1% HF mix. This produces a 10x dilution factor (dilution factor 2)

5.3. Total dilution factor is the product of the first and second dilution factors (i.e. 100 x 10 = 1000x dilution)

6. Reference and calibration solutions

6.1. 25 mL of 200 ppb indium and rhenium reference solution is required per 100 samples

6.1.1. 0.5 mL (1 ugg-1 In) + 0.005 mL (1000 ugg-1 Re) + 24.5 mL (5% $HNO_3$ + 0.1% HF mix)

6.2. 5mL of 0, 10, 20, 50, 200 and 500 ppb calibration solution are also required

6.2.1. Prepare 10 mL 500 ppb by weighing 0.5 mL of the two calibration solutions ('A' and 'B')[1] into 20 mL vial then adding 9.5 mL 5% $HNO_3$ + 0.1% HF mix. Record all weights

6.2.2. The other solutions can be made up from the 500 ppb solution

6.2.2.1. 0 ppb = 5mL 5% $HNO_3$ + 0.1% HF mix

6.2.2.2. 10 ppb = 0.1 mL 500 ppb solution + 4.9 mL 5% $HNO_3$ + 0.1% HF mix

6.2.2.3. 20 ppb = 0.2 mL 500 ppb solution + 4.8 mL 5% $HNO_3$ + 0.1% HF mix

6.2.2.4. 50 ppb = 0.5 mL 500 ppb solution + 4.5 mL 5% $HNO_3$ + 0.1% HF mix

6.2.2.5. 100 ppb = 1 mL 500 ppb solution + 4 mL 5% $HNO_3$ + 0.1% HF mix

6.2.2.6. 200 ppb = 2 mL 500 ppb solution + 3 mL 5% $HNO_3$ + 0.1% HF mix

6.2.2.7. 500 ppb = 5 mL 500 ppb solution

6.2.2.8. Record all weights

ELECTRON MICROPROBE (15KV, 20NA)

Thin sections from Stewart (1994) were analysed on the microprobe. Some had been previously run and still had their original carbon coating in good condition, others either had not been run previously or had had their carbon coating removed since then. In total, nine thin sections were analysed. Circles were drawn onto the back of the thin sections to mark areas of interest so that they could be easily found.

1. Load samples

1.1. Remove previous samples

1.1.1. "SX FIVE Control" window – "vacuum" tab – "sample exchange" button – "transfer the sample out of the chamber" option – follow instructions in pop up box

[1] Solution A: HPS-Q17617A is 10mg/L of Al, As, Ba, Be, Bi, Ca, Cd, Ce, Cs, Co, Cr, Cu, Dy, Er, Eu, Fe, Ga, Gd, Ho, La, Pb, Li, Lu, Mg, Mn, Na, Nd, Ni, P, K, Pr, Rb, Sc, Se, Sm, Sr, Tb, Th, Tl, Tm, U, V, Y, Yb, Zn in 2% $HNO_3$ Solution B: Cat#ICP-MS-68A Solution B is 10mg/L of Sb, Ge, Hf, Mo, Nb, Si, Ag, Ta, Te, Sn, Ti, W, Zr in 2% $HNO_3$ + Tr HF

1.1.2. Open transfer valve using the lever to the left of the sample-loading door by pushing in and sliding up. The lever will flick to the left at the top

1.1.3. flick the latch to the left so that the arrow on the top points out

1.1.4. release handle and slide slowly forward (spring loaded so needs to be held the whole time), slide back – watch through window to ensure sample plate comes back with it

1.1.5. close the valve by twisting the lever on the left to the right, then sliding it down

1.1.6. click “ok” on pop up window

1.1.7. wait for air lock to vent

1.1.8. push screw on left side of access door in and pull door back to open (swings right)

1.1.9. push sample plate to release, slide out and place on bench

1.1.10. close door

1.2. Put carbon coated thin sections on sample plate

1.2.1. Put latex gloves on

1.2.2. Have sample plate with hole in one end facing you

1.2.3. Slide previous thin sections out by pushing down gently and sliding up/ down

1.2.4. Slide new thin sections in with carbon coating facing up

1.2.5. Record sample numbers and order of thin sections on the plate (with first furthest away)

1.2.6. Stick carbon tape where two thin sections meet, ensuring that some tape also covers the edge of the sample plate to ensure thin sections do not move. Remove white backing of tape with tweezers

1.2.7. Overlay plastic grid on samples and record rough coordinates of where the marked circles are (x, y)

1.2.8. Remove grid before loading samples

1.3. Load new samples

1.3.1. Open access door and slide sample tray into place, hole end first, push until it clicks on (but don’t push so far that it releases)

1.3.2. Close door

1.3.3. “SX FIVE Control” window – “vacuum” tab – “sample exchange” button – “transfer the sample into the chamber” option – if door is properly closed, click “ok” to pump airlock” – follow instructions in pop up box

1.3.4. Open transfer valve with lever as above

1.3.5. Flick latch back up so that the arrow is pointing inwards

1.3.6. Slide handle forward and then back, watching through window to make sure sample plate does not come back out

1.3.7. Close transfer valve as above

1.3.8. Click “ok”

2. Turning electron beam on

2.1. “Beam and SEM setup” window – click “File” – select “load” from drop down menu – choose appropriate settings (in this case the first settings in the list were selected “hv15nA20”

2.2. Wait for beam to load

2.3. Go to “SX FIVE Control” window, select “Beam” tab. The diagram will show a red beam when the beam is finished loading. Can also check kV settings here

3. Navigating to circles

3.1. Go to “SX FIVE Control – Roller” window

3.2. Enter x- and y-coordinates obtained from the grid laid over the samples before loading into boxes labelled “X” and “Y”

3.2.1. Type the number, then press “Enter” on keyboard and wait for the stage to move before adding the next coordinate

3.3. In the same window, beam and light options are shown in the top right. Check Beam “Cut” and Scanning “Off”, then Light “On”

3.4. Press the button on the top right of the joystick control to auto focus

3.5. Return to same window and select Light “Off,” Beam “On” and Scanning “On.” A back-scatter image will now be visible in the top right screen

3.6. Use the joystick to navigate the back-scatter image to find the circle and desired area of analysis

4. Quick analysis to help identify minerals of interest

4.1. To obtain a quick look at what elements are present in a particular area, turn Scatter “Off” and go to the “Esprit” window and click “Acquire” button

4.2. Wait while data is acquired

4.3. A graph will be shown with peaks where a response has been recorded

4.4. Elements can be assigned to these peaks by clicking approximately in the centre of each peak and selecting the most likely element from the selection in the box in the top right corner of the graph

4.5. To return to navigating around the sample via back-scatter image, switch Scanning "On" and Beam "On" (Beam will automatically switch to "Cut" when finished acquiring

5. Saving a back-scatter image (Light "Off", Beam "On", Scanning "On")

5.1. Set the position of the image using the joystick navigation

5.2. Adjust focus and magnification as necessary using the knobs labelled "MAG." And "FOCUS"

5.3. Go to the "Acquire" window (left screen) – "Imaging" button – new window will open up – "Start Image" button

5.4. Wait for image to develop in the new window

5.5. Click "Save As" button – name the file identifying the image by sample number and circle number (e.g. EU1 circle1) – "Save"

5.6. Close the new window (click "No" when pop-up asks to save to probe database)

6. Choosing points for analysis and recording them

6.1. Navigate to desired area using joystick (Beam "On", Scanning "On", Light "Off)

6.2. Go to the "Automate" window – "Digitize" button – new window will pop up "Digitize Samples" – name the position in the "Unknown position name" box (name the same as the image i.e. sample number circle number) – "Add new unknown to position list" button

6.3. New position will appear in the "Position List" in "Automate" window

7. Choosing single points for analysis

7.1. Navigate to specific mineral/ point – in "Digitize Samples" window, select "Single Point(s)" button to record the location of the desired point of analysis (x- and y-coordinates will now appear in the "Automate" window

7.2. Repeat step (a) until desired number of points for the circle have been recorded

8. Choosing a grid of points for analysis

8.1. Instead of clicking "Single Point(s)" button, select "Rectangular Grid" button – new window will open

8.2. Set top left corner coordinates by navigating to a particular area and selecting the "Update Start" button in the new window

8.3. Set the bottom right corner coordinates by navigating to a point down and right of the starting point and click "Update Stop" button

8.4. Set grid step sizes in microns using the "X-step" and "Y-step" boxes

8.5. Click “ok” button

8.6. List of points will appear in the “Automate” window under the same unknown position name

9. Choosing points along a linear traverse

9.1. Instead of “Single Point(s)” button, select “Linear Traverse” button

9.2. As with selecting a grid of points, a new window will pop up and ‘Start’ and ‘Stop’ positions will need to be selected by navigating to them and clicking the appropriate “Update Start” or “Update Stop” button

9.3. Input the desired number of steps in the traverse into the “Traverse Steps” box

9.4. Click “OK”

9.5. A list of points will appear in the “Automate” window under the same unknown position name

10. To begin adding points to the next circle, navigate to it using the joystick and/or enter new x- and y-coordinates as appropriate. Repeat steps 3-6, followed by steps 7, 8, and/or 9 as desired.

11. To record points onto the back-scatter image

11.1. Have the current circle selected in the “Position List”

11.2. In “Digitize” window, select “Picture Snap” button. A new window will pop up

11.3. Open “File” drop down menu – “Load BMP Image” – select image file that corresponds to the open circle number – “Open”

11.4. In “Display” drop down menu, select “Digitized unknown position samples” and “Digitised position sample long labels” (a tick will appear to the left of each option to indicate they are activated)

11.5. Red circles and corresponding number labels will appear at approximately the same location on the open back-scatter image as they were on the actual back-scatter image (NB: coordinates may be slightly off in the saved image, but those selected based on the real-time back-scatter image will be in the correct position)

11.6. To save the back-scatter image with the points, open “File” drop down menu – select “Save as BMP (with graphics data)” – name file with the same sample number and circle number information, add ‘spots’ to the end to identify the image as one with the points information on it

12. To run full analysis of selected points

12.1. "Automate" window – select samples to analyse from the "Position List" by clicking and dragging up/down to the end of the currently loaded sample set – "Sample Setups" button, new window pops up – click "OK" – click "Yes" – returns to "Automate" window – select "Run Selected Samples" button – pop up gives estimated time to completion and asks for confirmation – click "OK"

XRF – FUSED DISCS

Method specific sample preparation:

1. Wash the glassware (vials, stopper lids) and crucibles. Enough crucibles for the number of samples, enough glass vials for the number of samples x3, enough lids for the number of samples x2

1.1. Using warm soapy water, a bottle brush and a cloth, wipe/gently scrub off any previous labelling and residues

1.2. Lay out each piece upturned on paper towel

1.3. Rinse each item in tap water, followed by deionised water. Rinsing with deionised water should be done three times

1.4. Place upturned on paper towel

1.5. Wipe out glass dishes

1.6. Place each vial upright in the glass dishes, with enough vials in each dish for the number of samples to analyse. Do the same with the crucibles

2. Dry glassware and crucibles for a minimum of 30-40 minutes at 110$^{o}$C

2.1. Place the dishes of vials and crucibles on the shelves in the oven

2.2. Lay out the lids on some paper towel on top of the oven. The heat from the oven will dry them. Do not place in oven as the plastic will go soft

3. Dry samples for at least 30-40 minutes at 110$^{o}$C

3.1. Takes vials with lip (no lid) out oven

3.2. Label vials with samples numbers

3.3. Scoop one slightly heaped spoonful of powdered sample into corresponding vial. Wipe spoon clean with tissue after each sample

3.4. Put vials with samples back into the dish and place on a shelf in the second oven

4. Weigh out samples into crucibles

4.1. Record sample number, crucible number, crucible weight to four decimal places

4.2. Tip each sample into one crucible, then weigh again and record the crucible + sample weight

4.3. Set filled crucibles out in silica trays ready to go into the furnace

5. Heat samples in furnace

5.1. Place silica trays with sample-filled crucibles into the furnace

5.2. Lock the door

5.3. Select appropriate program (2) – heat furnace at rate of 400$^{o}$C per hour until 900$^{o}$C, remains at 900$^{o}$C for three hours, cools

5.4. Leave program to run overnight

6. Remove samples from furnace and re-weigh

6.1. Allow samples to cool to room temperature in a decanter

6.2. Weigh crucible with sample in it. Record weight

6.3. Tip sample into a new (clean) glass vial and place stopper lid on. Label each vial as you go

6.4. Can now calculate L.O.I %

7. Dry x-ray flux in oven at 110$^{o}$C for at least two hours

8. Allow x-ray flux to cool to room temperature in a decanter

9. Measure out x-ray flux and sample into glass vials

9.1. Approx. 1g sample and 4g flux

9.2. Label new (clean) glass vial and lid

9.3. Place vial on scale. Tare scale

9.4. Add approx. 1g sample with a spatula. Record weight

9.5. Tare scale again

9.6. Add approx. 4g flux using different spatula. Record weight

9.7. Put on lid and mix sample and flux by gently tipping/ rolling the vial

9.8. Wipe spatulas clean with a tissue between each sample and keep flux in decanter when not using

10. Fused disc preparation

10.1. Contents of vial are now ready to be transferred to a Pt/5% Au crucible for fusion by heating above an oxy-propane flame (temp = 1100$^{o}$C)

10.2. Using Norrish-Chapman Prometheus Fusion Apparatus, crucible is heated for 10 minutes, until fusion is complete. The melt is the poured into a Pt/Au mould

and force cooled to room temperature using air 'jets' while the mould is still on the supporting ring

10.3. Sample disc is then labelled and ready for Whole Rock Analysis by XRF

11. Fused discs were taken to the CSIRO to run the Whole Rock Analysis

XRF – pressed pellets

Method specific sample preparation:

1. Weigh out sample powder and licowax binder into labelled glass vials

1.1. 6g sample + 1.5g binder

2. Cap vials and shake to mix powder and binder well
3. Use ethanol and tissue to clean components of pellet making equipment (see Figure 1)
4. Clean base first so that wall piece can be assembled onto it to avoid contamination after cleaning. Place stick top down on bench
5. Place an Al cup into the top of the wall piece. May need to use a cleaned spatula to push the cup down to the base
6. Carefully pour in mixed sample + binder into the Al cup
7. Slowly push stick in to avoid air pushing powder out
8. Place assembled pieces into the press (lift from base)
9. Lock valve by using the pole to turn the screw clockwise
10. Pump jack by hand until it becomes difficult
11. Place pole end in jack hole and pump until pressure on barometer at bottom left of press reads approx. 3
12. Leave for a few seconds before releasing the valve by using the pole to turn the screw anticlockwise
13. Press stage will slowly lower by itself, but can be sped up by pushing it down with your hands
14. Remove the pieces (lifting from the base) from the press and place on the bench
15. Lift the wall from the base – stick and Al cup will be lodged in the wall piece

15.1. To remove stick and Al cup, use the press as follows:

15.1.1. Place cloth on the press stage to unsure a soft landing for the Al cup (prevents damage to the pellet)

15.1.2. Place hollow metal tube on the tissue, with window hole facing you

15.1.3. Place wall and stick assembly onto the tube, with the Al cup at the bottom (it will fall out onto the cloth)

15.1.4. Lock the valve with the pole, and operate the press by hand until the stick is pushed into the wall far enough that the Al cup is released and falls down onto the cloth (will be able to see it through the window hole once is falls)

15.1.5. Release the valve and carefully remove the pieces

15.2. Label the base of the Al cup with a permanent marker

16. Clean the pieces with ethanol and tissue

16.1. To remove stick from wall cup, repeat Al cup removing procedure but with the stick and wall assembly up the other way, so the stick is pushed back through the wall

16.2. Place a piece of cloth between the stick and the top of the press to prevent damage to the internal parts of the equipment

16.3. Use ethanol to lubricate the stick and make its removal easier

16.4. May need to repeat the process in opposite directions multiple times until the stick is able to be pulled free

17. Repeat the process for each sample